



TALLINN UNIVERSITY OF TECHNOLOGY

SCHOOL OF ENGINEERING

Department of Electrical Power Engineering and Mechatronics

NOVEL BUCK-BOOST MICROINVERTER WITH ACTIVE DECOUPLING TECHNIQUE

UUDNE BUCK-BOOST MIKROINVERTER AKTIIVSE LAHTISIDUMISE TEHNIKAGA

MASTER THESIS

Student: Pavel Zõrjanov
/name/

Student code: 211915AAAM

Supervisor: Oleksandr Husev, Senior Researcher
/name, position/

Tallinn, 2023

(On the reverse side of title page)

AUTHOR'S DECLARATION

Hereby I declare, that I have written this thesis independently.
No academic degree has been applied for based on this material. All works, major viewpoints and data of the other authors used in this thesis have been referenced.

"....." 202.....

Author:
/signature /

Thesis is in accordance with terms and requirements

"....." 202....

Supervisor:
/signature/

Accepted for defence

".....".....2023.

Chairman of theses defence commission:
/name and signature/

Non-exclusive Licence for Publication and Reproduction of Graduation Thesis¹

I, Pavel Zõrjanov hereby

1. grant Tallinn University of Technology (TalTech) a non-exclusive license for my thesis
Novel Buck-Boost microinverter with active decoupling technique,
(title of the graduation thesis)

supervised by Oleksandr Husev,

(Supervisor's name)

1.1 reproduced for the purposes of preservation and electronic publication, incl. to be entered in the digital collection of TalTech library until expiry of the term of copyright;

1.2 published via the web of TalTech, incl. to be entered in the digital collection of TalTech library until expiry of the term of copyright.

1.3 I am aware that the author also retains the rights specified in clause 1 of this license.

2. I confirm that granting the non-exclusive license does not infringe third persons' intellectual property rights, the rights arising from the Personal Data Protection Act or rights arising from other legislation.

14.05.2023

¹ The non-exclusive licence is not valid during the validity of access restriction indicated in the student's application for restriction on access to the graduation thesis that has been signed by the school's dean, except in case of the university's right to reproduce the thesis for preservation purposes only. If a graduation thesis is based on the joint creative activity of two or more persons and the co-author(s) has/have not granted, by the set deadline, the student defending his/her graduation thesis consent to reproduce and publish the graduation thesis in compliance with clauses 1.1 and 1.2 of the non-exclusive licence, the non-exclusive license shall not be valid for the period.

ABSTRACT

Author: Pavel Zörjanov

Type of the work: Master Thesis

Title: Novel buck-boost microinverter with active decoupling technique.

Date: 14.05.2023

76 pages

University: Tallinn University of Technology

School: School of Engineering

Department: Department of Electrical Power Engineering and Mechatronics

Supervisor(s) of the thesis: Senior Researcher Oleksandr Husev

Consultant(s): -

Abstract:

The aim of this thesis is to review various microinverter topologies and types of active decoupling circuits, as well as to compare and analyze different control strategies. The thesis work will compare three control strategies for a microinverter filtering unit in terms of component volume, power density, cost, and losses.

The experimental part of this thesis work will be conducted using PSIM simulation software, and the data will be analysed using internal tools in PSIM software as well as software such as Microsoft Excel.

Work consists of 5 main parts: theoretical part, calculation part, control strategy part, experimental results and simulation verification part and analysis of simulation results.

Keywords: decoupling, capacitor, control, PSIM, microinverter

LÕPUTÖÖ LÜHIKOKKUVÕTE

Autor: Pavel Zõrjanov

Lõputöö liik: Magistritöö

Töö pealkiri: Uudne buck-boost mikroinverter aktiivse lahtisidumise tehnikaga.

Kuupäev:
14.05.2023

76 lk

Ülikool: Tallinna Tehnikaülikool

Teaduskond: Inseneriteaduskond

Instituut: Elektroenergeetika ja mehhatroonika instituut

Töö juhendaja(d): vanemteadur Oleksandr Husev

Töö konsultant (konsultandid): -

Sisu kirjeldus:

Selle lõputöö eesmärk on uurida erinevaid mikroinverterite topoloogiaid ja aktiivse lahutusahela tüüpe, samuti võrrelda ja analüüsida erinevaid juhtimisstrateegiaid. Töö võrdleb kolme juhtimisstrateegiat mikroinverteri filtrimisüksuse puhul komponentide mahtuvuse, võimsustiheduse, maksumuse ja kadude osas.

Töö eksperimentaalne osa viiakse läbi PSIM simulatsioonitarkvara abil ja andmeid analüüsitakse PSIM tarkvara sisemiste vahendite ja tarkvara, näiteks Microsoft Excel, abil.

Töö koosneb 5 osast: teoreetiline osa, arvutuslik osa, juhtimisstrateegia osa, eksperimentaalne osa ning tulemuste analüüs.

Märksõnad: lahtisidumine, kondensaator, juhtimine, PSIM, mikroinverter.

THESIS TASK

Thesis title in English:	Novel buck-boost microinverter with active decoupling technique
Thesis title in Estonian:	Uudne buck-boost mikroinverter aktiivse lahtisidumise tehnoloogiaga
Student:	Pavel Zõrjanov, 211915AAAM
Programme:	Energy Conversion and Control Systems
Type of the work:	Master Thesis
Supervisor of the thesis:	Oleksandr Husev
Co-supervisor of the thesis: (company, position and contact)	
Validity period of the thesis task:	2022/2023 2022/2023 Spring
Submission deadline of the thesis:	18.05.2023

Student (signature)

Supervisor (signature)

Head of programme
(signature)

Co-supervisor (signature)

1. Reasons for choosing the topic

Active decoupling technique is not researched a lot yet. This thesis work will research and review how to implement this technique to modern inverter and how to control it.

2. Thesis objective

The aim of this thesis is to make a working model of compact microinverter with high power density.

3. List of sub-questions:

- To analyze existed methods of power density increasing techniques
- To analyze active decoupling technology
- To implement an active decoupling technique to controller

4. Basic data:

Basic data is information got from literature observation and calculated results used in simulation.

5. Research methods

Literature analysis and simulation model based on calculation results.

Simulation data analysis using Excel.

6. Graphical material

- Simulation schemes
- Simulation results
- Graphical analytics

Graphical elements will be also included in the appendixes.

7. Thesis structure

- Review of existed methods of power density increasing techniques
- Selection of basic microinverter
- Implementation of active decoupling technique to controllers
- Simulation
- Simulation results and analytics

8. References

Mainly research articles and reports

Main references:

- *ieeexplore.ieee.org*
- *researchgate.net*
- *sciencedirect.com*
- *scholar.google.com*

9. Thesis consultants

-

10. Work stages and schedule

Going through the literature (31.12.2022)

Simulation model (31.12.2022)

Theoretical part (12.02.2023)

Practical part (01.04.2023)

Completing the first version of the work (01.05.2023)

Completing the final version of the thesis (11.05.2023)

TABLE OF CONTENTS

ABSTRACT	4
LÕPUTÖÖ LÜHIKOKKUVÕTE	5
THESIS TASK	6
PREFACE	10
LIST OF ABBREVIATIONS AND SYMBOLS	11
INTRODUCTION	12
THEORETHICAL PART	14
1.1 A review of different types of microinverters	14
1.1.1 Two-stage microinverters	14
1.1.2 Single-stage microinverters	15
1.1.3 Maximum Power Point Tracking	16
1.2 Conventional power decoupling	16
1.3 Active power decoupling technique	18
1.4 Active power decoupling topologies	18
1.4.1 Independent topologies	19
1.4.2 Dependent topologies	22
1.5 Review and analysis of existed topologies	22
1.5.1 Conventional flyback microinverter	22
1.5.2 Interleaved flyback microinverter	23
1.5.3 Buck-Boost microinverter topology	24
1.5.4 Boost type microinverter topology	27
1.6 Review of different capacitor types	28
2. SELECTED MICROINVERTER TOPOLOGY	31
2.1 Active power decoupling circuit and parameters calculation	33
2.1.1 Active power decoupling circuit working mode	35
2.1.2 Active power decoupling circuit	37

3. CONTROL STRATEGY.....	39
3.1 Fast Fourier Transform	39
3.2 Proposed control strategy	40
3.2.1 Proposed control scheme	41
3.3 Control strategy 2.....	41
3.3.1 Control scheme.....	44
3.4 Control strategy 3.....	46
3.4.1 Control scheme.....	47
4. EXPERIMENTAL RESULTS AND SIMULATION VERIFICATION	48
4.1 Experimental results of proposed control strategy.....	48
4.2 Experimental results of control strategy 2.....	52
4.3 Experimental results of control strategy 3.....	55
5. ANALYSIS OF SIMULATION RESULTS AND COMPONENTS SELECTION	59
5.1 Components selection	60
5.2 MOSFET power losses.....	64
5.2.1 Conduction losses calculation.....	64
5.2.2 Switching losses calculations	66
5.2.3 Analysis of calculated losses	66
SUMMARY.....	68
KOKKUVÕTE	70
LIST OF REFERENCES	72

PREFACE

The focus of my research is active power decoupling technique and its implementation in microinverters, a subject that has been of great interest to me for some time.

In writing this thesis, goal was not only to provide a comprehensive overview of the existing literature but also to simulate working of different control strategies.

I would like to express my gratitude to my thesis advisor for their guidance, support, and invaluable feedback throughout the process.

LIST OF ABBREVIATIONS AND SYMBOLS

ESR – Equivalent Series Resistance

PDC – Power Decoupling Circuit

PPD – Passive Power Decoupling

APD – Active Power Decoupling

PWM – Pulse Width Modulation

PV – Photovoltaics

FFT – Fast Fourier Transform

DFT – Discrete Fourier Transform

INTRODUCTION

In recent years, there has been a growing interest – especially in Estonia, in decentralized power generation and distribution systems, such as photovoltaic (PV) systems.

There are several issues associated with the use of solar microinverters in modern PV systems. Most modern solar inverters use traditional technologies based on passive components, which have a major drawback of overheating when not using active cooling systems. This can result in frequent errors and reduced efficiency.

The efficiency of solar microinverters is crucial for the functionality of the PV system, as microinverters are typically installed together with the PV panels on the roof, making it difficult to maintain the system. To maximize the efficiency and reliability of these systems, it is important to have high-performance power converters that can effectively manage the flow of power from the PV panels to the load. One potential solution to increase efficiency is the use of an active decoupling technique, which replaces passive components in the filter part with active components.

Buck-boost microinverters are a type of power converter that have gained popularity in PV systems due to their ability to operate with a wide input voltage range and provide high-quality output voltage. However, traditional microinverters that work in buck-boost diapasons are subject to output voltage ripple, which can reduce the overall performance of the system and lead to power losses.

In this master thesis project, I aim to address this issue by proposing a novel microinverter that incorporates an active decoupling technique. The active decoupling technique uses active components as a filter what leads to improving the performance of the converter. By combining this technique with the benefits of the microinverter, proposed microinverter has the potential to provide high-quality output voltage, increased efficiency, and improved reliability for PV systems.

This thesis will provide a comprehensive investigation of the design, implementation, and evaluation of the microinverter with active decoupling technique. The results of this research will contribute to the advancement of power conversion technology for decentralized power generation and distribution systems and offer practical insights for the design and implementation of similar systems in the future.

The main focus of this thesis will be on the following topics:

- Theoretical part – An overview and comparison of various microinverter topologies that exist today, a theoretical overview of the active decoupling

technique, and the calculation of necessary components for proper converter functionality.

- Experimental part – Simulation of the working process of the microinverter with active decoupling technique using PSIM simulation software.
- Analysis – A comparison of theoretical and experimental results, followed by an analysis of the suitability of the microinverter for real-life performance.

THEORETHICAL PART

1.1 A review of different types of microinverters

Photovoltaic (PV) microinverters are power conditioning systems that convert DC power from solar panels into AC power suitable for the electrical grid. There are several main types of PV microinverters: single-stage and multi-stage. The type of microinverters used affects the control strategies required to achieve proper grid connection.

This part of master thesis work will give a brief overview of different types of buck-boost microinverters existed today. Both: single- and multi-stage can be either galvanically isolated or not.

1.1.1 Two-stage microinverters

In a grid-connected system with multi-stage topologies, two stages are used to perform specific tasks. The first stage involves using a DC-DC converter to extract the maximum power from the PV panel and amplify the voltage. The second stage uses an inverter to inject high quality current to the utility grid. [1]

The DC-DC converter in the multi-stage topology is typically a boost type converter that provides the necessary voltage amplification at the DC link, thereby reducing the capacitance value and increasing the life span of the micro-inverters. [1]

One popular topology is a two-stage micro-inverter with a flyback converter in the first stage for voltage amplification and galvanic isolation, and a full bridge inverter in the second stage for AC current injection. However, this topology suffers from high switching losses due to the hard switching of all power MOSFETs.

Although using a two-stage configuration is a relatively simple power conversion technique, it does have some significant limitations. The main limitations include size and efficiency issues that may hinder the ability to connect a PV panel to the utility grid. With two stages of power conversion, the efficiency is naturally reduced, and the converter's power density is also compromised. Another drawback of this configuration is that achieving ZVS for the second stage of the converter is challenging, so a low switching frequency PWM inverter is typically used to minimize switching losses. However, using a low switching frequency result in the need for a bulky and inefficient filter to eliminate the high frequency component and inject high quality current into the grid. [1]

Another challenge faced by a two-stage microinverter is managing the power interface during the transfer of DC power from the solar module to the AC-grid side. A DC link capacitor is used in parallel between the first and second stages to balance out the power difference and ensure optimal performance.

1.1.2 Single-stage microinverters

Single-stage topology is most modern type of topology, it aims to improve system efficiency by reducing the number of components needed for maximum power point tracking (MPPT) control, voltage regulation, and DC to AC conversion. However, one of the drawbacks of eliminating the DC-DC stage is that a large capacitance is needed for power decoupling.

If for multi-stage topology a DC-link capacitor is used between two stages, in single-stage topology power decoupling is completed by using capacitor in parallel with PV input. The overall efficiency and reliability of a single-stage PV system can be affected by several obstacles related to this electrolytic capacitor. This component is typically characterized by a large size, short lifespan, large tolerance (up to $\pm 20\%$), and dependence on temperature. [2]

There is a lot of different topology exists nowadays. Many of them are derivatives from four main topologies [1]:

- Buck-boost topology – transformer-less microinverter that uses LC-filter to reduce the current harmonics that arise due to semiconductor switching.
- Flyback topology - this topology uses a circuit isolation by integrating a line frequency transformer between the PV and the grid. For a smoother AC output, an LC-filter is used between PV and the grid. However, the conventional flyback topology experienced reduced output power performance due to the high switch stress caused by the leakage inductance of the transformer. [2]
- Double boost topology –transformer-less topology enables operation in both waveforms by using a mirrored circuit on both the right and left sides. The conventional boost topology circuit results in additional switching losses due to the high-frequency switching of the device. Furthermore, the voltage gain is limited by the duty cycle of the conventional double-boost microinverter, resulting in lower instantaneous output AC compared to input DC.

1.1.3 Maximum Power Point Tracking

Maximum Power Point Tracking (MPPT) is an important technology used in solar power systems. It is a method used to maximize the amount of power that can be extracted from a solar panel. This technology is especially important for large-scale solar installations where maximizing efficiency and output is critical.

MPPT technology works by continuously tracking the maximum power point (MPP) of the solar panel, which is the point at which the panel produces the maximum amount of power. The MPP is affected by many factors, including temperature, irradiance, and shading. By tracking the MPP, MPPT controllers can adjust the voltage and current to ensure that the maximum power is always being extracted from the panel. [16]

One of the main advantages of MPPT technology is that it can significantly increase the efficiency of a solar power system. When a solar panel is not operating at its maximum power point, some of the energy produced is lost. MPPT technology ensures that the panel is always operating at its MPP, which means that more of the energy produced is being used. This results in higher energy yields and lower overall costs. [16]

Another advantage of MPPT technology is that it can improve the performance of solar panels in low-light conditions. In low-light conditions, the voltage and current output of a solar panel can drop significantly, which can lead to a significant reduction in energy output. MPPT technology can help to mitigate this issue by adjusting the voltage and current to ensure that the panel is always operating at its MPP. [16]

The main disadvantage of a maximum power point tracking system is that a complex control algorithm is needed to achieve maximum efficiency. A control system complexity can be increased if some sophisticated topology or filtering circuit is added. Some of control strategies are: Fixed Duty Cycle, Constant Voltage, perturb & observe and perturb & observe based on PI regulator, incremental conductance, temperature method and others. [16, 17]

1.2 Conventional power decoupling

For a grid connector inverter, the output power could be described by following equation that consist of two parameters – average output power and pulsating power [4]:

$$P_{out} = \frac{1}{2}U \times I + \frac{1}{2}U \times I \times \cos(4\pi ft) \quad (1.1)$$

where P_{out} – output power,
 U – grid voltage,
 I – injected current,
 f – grid frequency,
 t – time.

As it is seen from equation 1.1, pulsating component is characterized as a fixed double-grid frequency component, so it is possible to eliminate this component by using passive filters. Conventionally is electrolytic capacitor used for this purpose. Power decoupling capacitor is placed in parallel with PV input or within the stage of microinverter. Capacitance of decoupling capacitor can be calculated according to next equation [4]:

$$C = \frac{P_{DC}}{2\pi f U_{DC} \Delta u} \quad (1.2)$$

where P_{DC} – output power of PV system,
 U_{DC} – voltage across capacitor,
 Δu – voltage ripple.

A lot of topologies are proposed for the best efficiency of implementation decoupling capacitor in microinverter systems. In this thesis work different topologies will not be reviewed, focus will be made only on placing of decoupling capacitor in converter.

PV-side decoupling – decoupling capacitor is placed in parallel with PV input. This means that the capacitance of decoupling capacitor is very high according to equation 1.2. It is due to relatively low voltage from PV input. Increased size of capacitor makes the whole microinverter size bigger, so power density is not optimal. The second drawback of high decoupling capacitance is reduced efficiency due to power losses. [4] [6]

DC-link decoupling – decoupling capacitor is placed between the stages of microinverter. In this case capacitor is working with higher voltage so it allows to decrease capacitance and therefore the size of capacitor. Together with decreasing capacitance a higher voltage ripple will be across the DC-link capacitor what can lead to change of output current waveform. Some sophisticated control techniques should be used to solve this problem, as a result the whole converter becomes larger and complicated. [4][7]

AC-side decoupling – decoupling capacitor is placed in the AC-side of converter, usually embedded in inverter stage. Main advantage of this method is that capacitor with small capacitance can be used. The second advantage is because of working with alternative current a non-polarized capacitor could be used. Film non-polarized capacitors are known for their higher stability, lower dielectric absorption, leakage current, and ESR compared to electrolytic ones. They can operate at high temperatures and are less prone to failure due to age or environmental factors [5]. In case of using this type of decoupling, a bi-directional switch must be applied. [4][7]

To sum up, the passive decoupling methods are not the best choice if high power density, high lifetime, and possibility of working at high temperatures is needed.

1.3 Active power decoupling technique

Traditional microinverter topologies are using some filtering components for proper functionality of inverter. As it is written in previous part, most popular filtering opportunity is using of DC-link capacitor. DC-link capacitor is best low-cost choice to minimize voltage ripple, but a lot of problems is connected to using this capacitor – mainly these capacitors have high losses caused by their equivalent series resistance or ESR, as well as their short lifetime.

As an alternative to DC-link capacitor is possible to apply active decoupling technique that uses capacitive component together with switching elements such as transistors. Active decoupling can be used in both DC-DC and DC-AC stages and includes a capacitor that cycles the AC ripple component [3].

The active decoupling technique comprises of decoupling circuit topologies and control algorithms. The control algorithms are categorized into two types: open-loop control method and closed-loop control method. The open-loop control method is commonly used due to its simplicity, but it is prone to parameter variations. On the other hand, the closed-loop control method can deliver excellent performance even in the presence of disturbances, but designing a stable closed-loop control algorithm can be challenging at times. [8]

1.4 Active power decoupling topologies

This section will provide an overview of the APD topologies that have been proposed in single-phase systems, highlighting their operating principles, advantages, and limitations.

In active power decoupling systems, a special decoupling cell is used to eliminate voltage ripple. Decoupling cell can be connected to main converter in parallel, in series or other way – for example differentially. Decoupling cells can be either voltage source- or current source oriented and both of energy storage components could be used: a capacitor or an inductor. [7][8]

In voltage source oriented basic cells, the DC voltage is considered as the main quantity, and it is controlled and regulated by the power converter. Mainly a capacitor is used as an energy storage component. Inductor as an energy storage component seems to be worse than capacitor because of its higher cost and volume. [8]

In current source oriented basic cells, the DC current is considered as the main quantity, and it is controlled and regulated by the power converter. In this case also a capacitor used for storing an energy. [8]

Active power decoupling topologies can be divided in two main categories: independent APD topology and dependent APD topology.

1.4.1 Independent topologies

Independence of APD topologies means that the single-phase converters and the basic decoupling cells operate independently of each other. Typically, the basic decoupling cell is connected to the DC link of the single-phase converters in either parallel or series. The single-phase converter regulates the DC-link voltage/current, while the basic decoupling cell deals with the ripple power. The incorporation of an additional basic decoupling cell does not affect the operation point of the original single-phase converter. Moreover, the control methods and modulation strategies for both the original single-phase converter and the basic decoupling cell can be designed independently of each other. [8]

Buck topology uses low voltage capacitor to eliminate voltage ripple. The decoupling capacitor voltage should be lower than DC-link voltage, that makes it a good choice when system voltage is high [8]. The capacitor is controlled to eliminate the second order ripple by regulating its charging and discharging. A DC voltage offset is needed for the efficient control and tracking of high-order harmonics in an underdamped system. As a drawback, the capacitor voltage does not completely discharge every cycle, indicating that the capacitor is not fully utilized. [3]

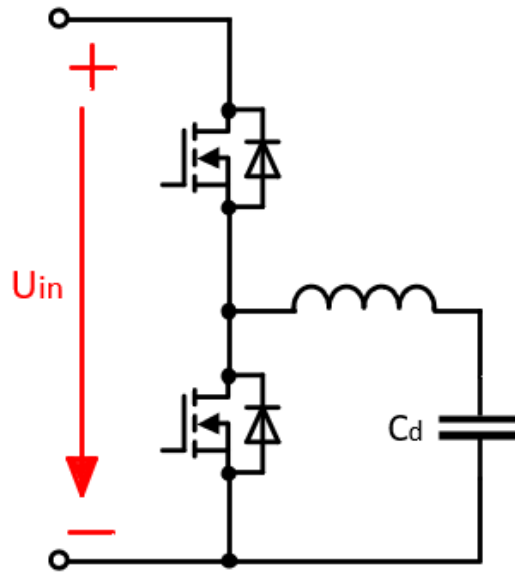


Figure 1.1 Buck topology for active power decoupling circuit

Boost topology uses high voltage capacitor to eliminate voltage ripple. This topology is the most used nowadays. In this case a capacitor must be larger because it doesn't only eliminate AC voltage ripple, but it also carries a DC voltage. As a result of working with higher voltage than in case of buck topology, all the switching components must be also suitable. This increases the total size of the converter. [3, 8]

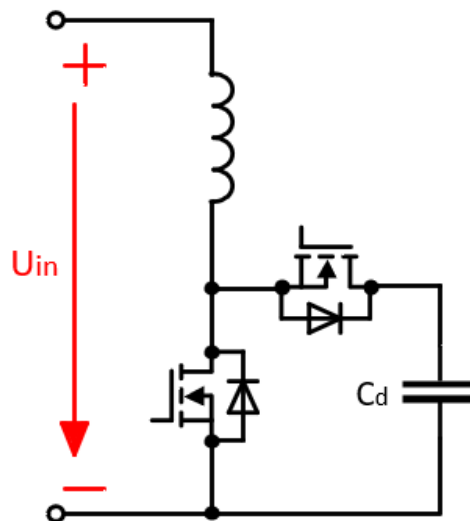


Figure 1.2 Boost topology for active power decoupling circuit

Buck-boost topology in which capacitor voltage can be regulated to be either lower or higher than input voltage. So in this case many advantages of buck and boost topologies can be used. [9]

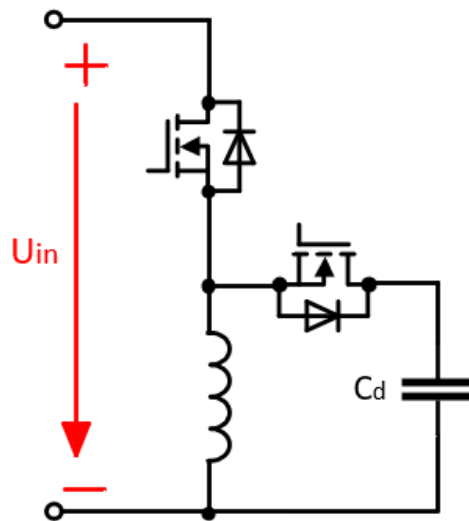


Figure 1.3 Buck-boost topology for active power decoupling circuit

H-bridge topology uses small capacitor in filtering part of AC side, so it helps to control reactive power. In this case capacitor is used only to eliminate voltage ripple on AC side, so it stores minimal amount of voltage and therefore the size of capacitor is optimal. In this case the capacitor voltage should be sine wave or full-wave rectified sine wave. [8]

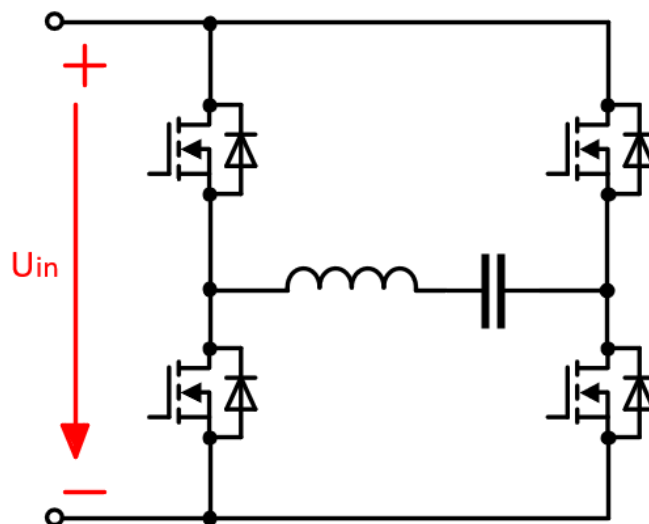


Figure 1.4 Full bridge topology for active power decoupling circuit

1.4.2 Dependent topologies

In case of dependent active power decoupling topologies, a power semiconductor device is shared with the main converter. As the decoupling circuit is integrated with the main converter circuit, the control methods and modulation strategies for both circuits are tightly coupled. This results in more complex control algorithms and modulation techniques, which can be difficult to design and implement.

Dependent systems can also use similar topologies to independent ones when sharing a bridge arm between a decoupling cell and a main converter part. H-bridge topology could be used also in dependent system if sharing lower switches with converter itself. Also, all aforementioned topologies could be used in dependent system if connected differentially. [8]

Converters with dependent topologies consist of fewer components but more complex control technique must be used to utilize components maximally. [10]

1.5 Review and analysis of existed topologies

1.5.1 Conventional flyback microinverter

The conventional flyback microinverter is a popular choice for small-scale renewable energy systems. It is a DC-AC converter that can convert the DC output of a renewable energy source into a form suitable for AC grid.

The conventional flyback microinverter consists of four main components: an input filter, a DC-DC stage, and an output filter. The input filter is used to smooth the DC input and reduce any high-frequency noise or ripple. The DC-DC converter is used to step up or step down the DC voltage to a level suitable for the inverter stage. The output filter is used to smooth the AC output waveform and reduce any harmonic distortion or noise.

During the on-state of the primary switch S_{PV} , the full DC voltage of PV panel is going through the transformer causing the magnetizing inductance to accumulate energy and increase its magnetizing current. When S_{PV} switches off, the energy stored in the transformer's magnetizing inductance is transmitted to the output. As the output is AC, it passes through either D_{AC1} and S_{AC1} when the output voltage is positive or through D_{AC2} and S_{AC2} when it is negative.

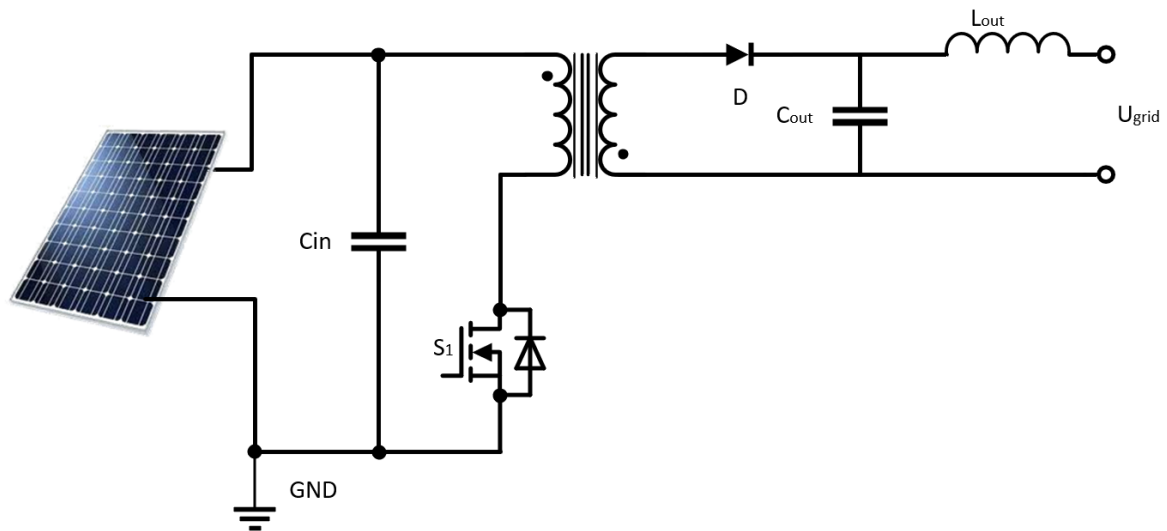


Figure 1.5 Conventional flyback converter topology (only DC stage) [21]

As it was reviewed previously, the main problem is that the maximum power extracted from the PV module must remain constant even when power flow to the grid varies over time, in order to maximize power harvest operation. As a result, an instantaneous mismatch occurs between the PV power and the AC power fed into the grid. To mitigate this issue, a large electrolytic capacitor is required to be connected between the PV module and microinverter for balancing this power difference. [21]

Additionally, in high temperature conditions such as in the summer season, the lifetime of electrolytic capacitors is shortened, leading to a shorter lifespan for the micro-inverter. Therefore, to transfer high power, a large capacitance of an electrolytic capacitor is needed. This ultimately increases the total cost of the micro-inverter and reduces its efficiency. [21]

1.5.2 Interleaved flyback microinverter

Interleaved flyback inverters are a type of power electronic converter that have gained popularity in recent years due to their high efficiency, low cost, and ease of control. The interleaved flyback topology involves connecting multiple flyback converters in parallel to increase the overall power output and reduce the ripple current and voltage across the input and output.

Interleaved flyback converters operate on the principle of parallel connection of multiple converters, also known as "phases". These phases are interleaved with each other. For instance, when two converter phases are employed, they are operated 180° out of phase with respect to one another. This means that the primary switch of each converter

receives the same gating signal as the other, but it is shifted by 180° in the switching cycle. [52]

The key advantage of interleaved flyback inverters is their ability to distribute the input and output current across multiple converters, resulting in reduced current and voltage stress on each converter. This, in turn, leads to higher efficiency, lower cost, and increased reliability. The parallel connection of the converters also results in a reduced ripple current and voltage, which improves the overall system performance. [52]

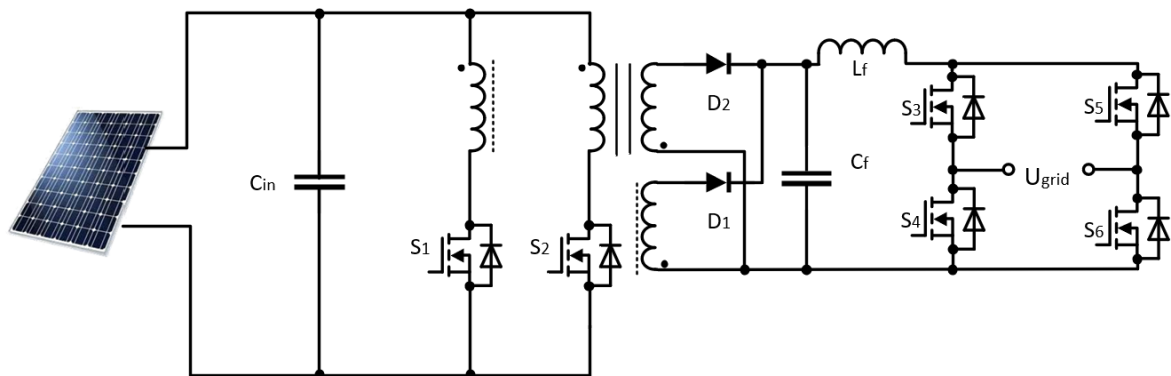


Figure 1.6 Interleaved Flyback microinverter topology [52]

Interleaved flyback inverters have several design considerations that must be taken into account to ensure proper operation. One of the key considerations is the selection of the number of converters to be connected in parallel. The number of converters is usually chosen based on the required power output, with more converters providing higher power output but also increasing the complexity of the control system. [52]

Another important consideration is the design of the interleaving control scheme, which determines the timing and phase shift of the converters. The interleaving control scheme is critical to ensuring proper distribution of the input and output current across the converters, and to reducing the ripple current and voltage.

1.5.3 Buck-Boost microinverter topology

A buck-boost microinverter is another type of DC-AC converter used in photovoltaic (PV) systems. It is similar to the flyback microinverter in that it converts the DC voltage from the PV panel into AC voltage for grid-tied applications. However, it uses a different topology and has some distinct differences compared to the flyback microinverter.

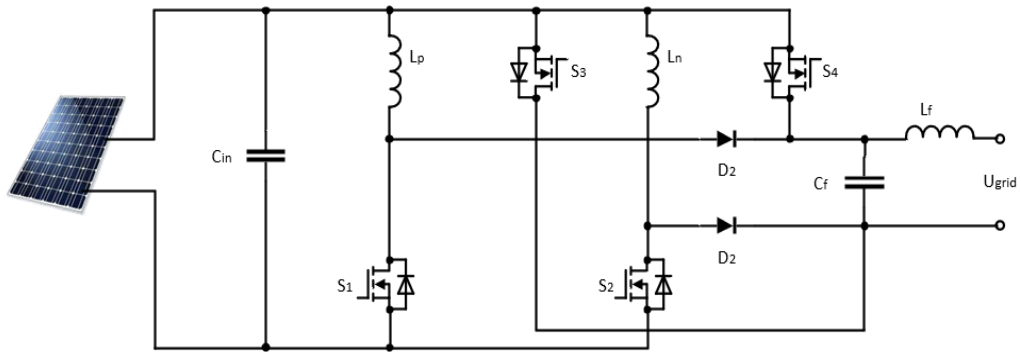


Figure 1.7 Buck-Boost microinverter topology. [24]

In a buck-boost microinverter, the DC input voltage can be higher, lower, or equal to the AC output voltage. This is achieved by using a combination of a buck converter and a boost converter, which are connected back-to-back. During the first half-cycle, the buck converter steps down the DC input voltage to a lower level, and during the second half-cycle, the boost converter steps up the voltage to a higher level. This allows for a wider range of input voltages to be converted to a fixed output voltage.

This topology proposes 6 different working modes: three of them occurs at the positive half of the cycle and another three at the negative half of the cycle. Working principle is quite similar to conventional DC-DC buck-boost converter but contains additional component that help to generate an AC output voltage. [24]

- Mode 1: SW_1 is on for this working condition, so current is applied to L_p and magnetizes it. Leakage current is stopped from flowing through the path because the impedance of that path is high. [24]

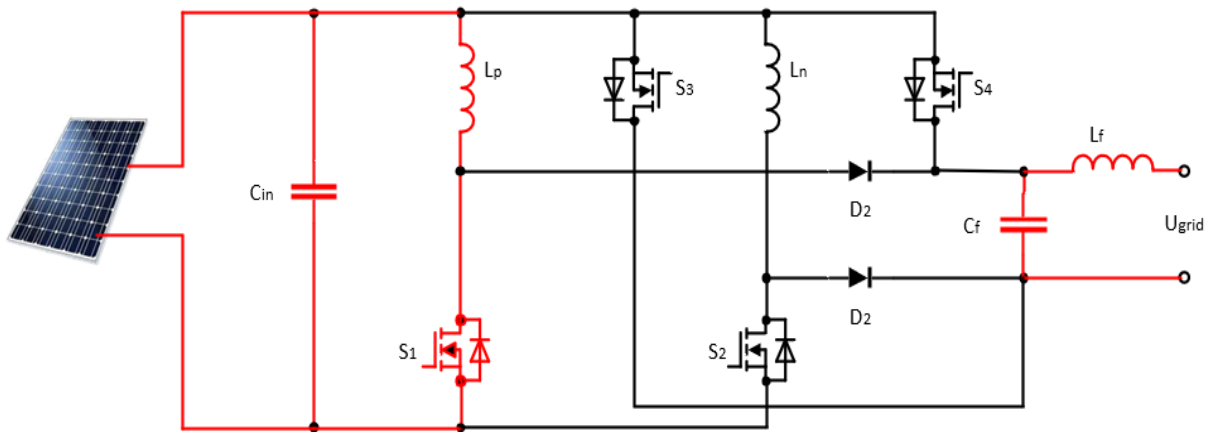


Figure 1.8 Working mode 1 of Buck-Boost microinverter

- Mode 2: After storing sufficient energy in inductor L_p to attain the required voltage gain, the second operating mode starts. During this mode, the stored energy is discharged to the filter capacitor and load. SW_1 is turned off, while diode D_p becomes forward-biased and creates a conduction path through SW_3 and inductor L_p . [24][25]

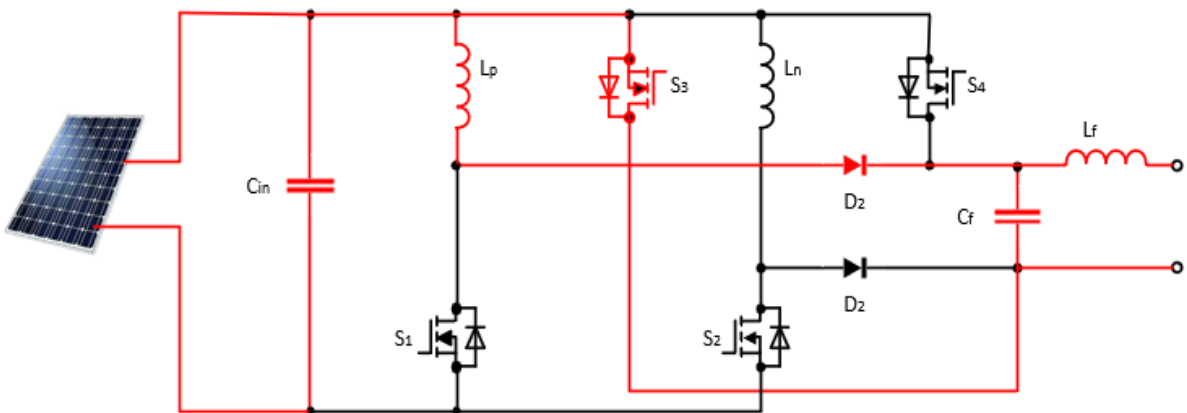


Figure 1.9 Working mode 2 of Buck-Boost microinverter

- Mode 3: The third mode starts once all the energy in the inductor L_p is transferred to the capacitor C_f . During this mode, the energy from the output filter capacitor is transferred to the load. [24]

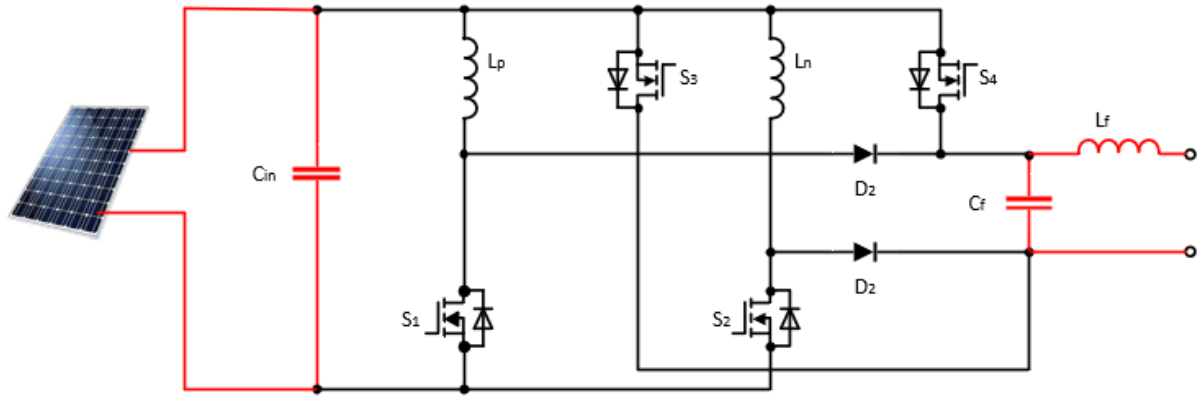


Figure 1.10 Working mode 3 of Buck-Boost microinverter

It must be noted that in this topology only one switch conducts current at the moment, even if other switch is also in ON-state. This leads to decreasing switching losses.

One advantage of the buck-boost microinverter is that it can be more efficient than the flyback microinverter, especially when the DC input voltage is lower than the AC output voltage. This is because the flyback converter stores energy in the transformer during the on-time of the primary switch and then releases it during the off-time. This energy transfer can cause significant losses in the transformer and the output diodes, especially when operating at high frequencies. In contrast, the buck-boost converter does not store energy in the same way, so it can be more efficient in certain operating conditions.

However, the buck-boost microinverter is more complex and expensive to design and build compared to the flyback microinverter. It requires more switches and more inductors and capacitors, which increases the overall size and cost of the system. In addition, the control circuitry for the buck-boost converter is more complex, which can make it more difficult to implement and optimize.

1.5.4 Boost type microinverter topology

At its core, the Boost topology is a type of DC-DC converter that uses a boost converter to step up the DC voltage from the solar panels to a higher voltage level that is suitable for conversion to AC power. [26]

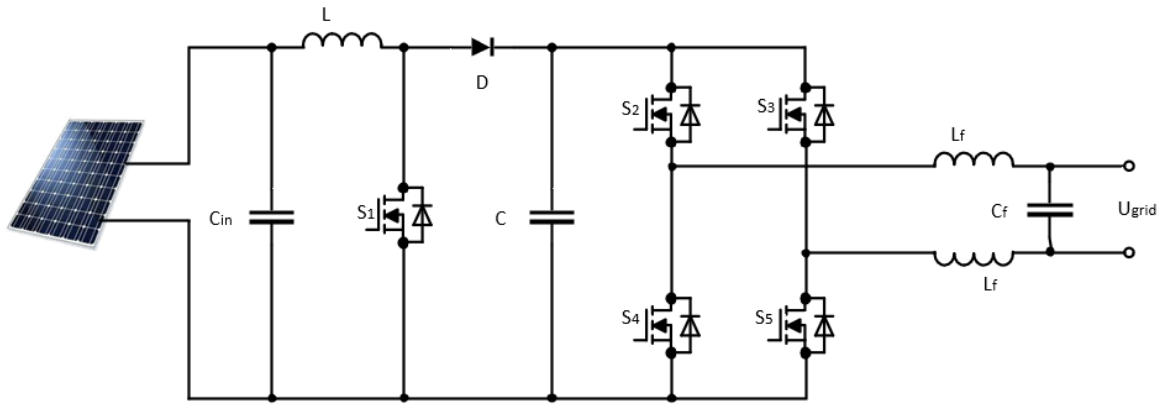


Figure 1.11 Buck microinverter topology

One of the primary advantages of the Boost topology is its ability to operate at higher voltage levels than other types of microinverters. This allows for longer wire runs between the solar panels and the inverter, which can be particularly useful for large installations or installations in areas with a lot of shade.

Another advantage of the Boost topology is its ability to handle a wide range of input voltages and power levels. This makes it a flexible solution for a variety of different solar panel configurations and can help to optimize power output under different weather conditions.

However, one potential disadvantage of the single-stage Boost topology is that it requires more complex control circuitry than other types of microinverters. This can make the Boost topology more expensive and potentially less reliable than simpler microinverter designs. [27]

1.6 Review of different capacitor types

Capacitors are an essential component of power electronics especially in the field of power filters, and there are different types of capacitors available, each with its unique characteristics. Here's a comparison of the most used capacitor types in power electronics:

- Electrolytic Capacitors:

Electrolytic capacitors are polarized capacitors that use an electrolyte as a dielectric. They are widely used in power electronics due to their high capacitance and ability to handle high voltages. They have a relatively large physical volume and a relatively short lifespan compared to other capacitor types. They also have a lower tolerance and are

more sensitive to temperature variations. However, electrolytic capacitors are relatively inexpensive compared to other types and are commonly used in power supply filters. [41]

- Tantalum Capacitors:

Tantalum capacitors are a special case of electrolytic capacitors, also polarized capacitors, but they use tantalum as a dielectric. They have a relatively high capacitance and a small physical size compared to electrolytic capacitors. Tantalum capacitors are commonly used due to their high reliability, stability, and ability to handle high temperatures. However, they are more expensive than other types of capacitors and are sensitive to voltage spikes, which can cause them to fail catastrophically. [41][42]

Compared to electrolytic capacitors, tantalum capacitors have a smaller physical size and a longer lifespan. However, they are more expensive.

- Ceramic Capacitors:

Ceramic capacitors are non-polarized capacitors that use a ceramic material as a dielectric. They are widely used in power electronics due to their small physical size, high capacitance, and ability to handle high voltages. They have a relatively long lifespan compared to electrolytic capacitors and are less sensitive to temperature variations. However, they have a lower tolerance and are more sensitive to voltage variations. [41]

- Film Capacitors:

Film capacitors are non-polarized capacitors that use a thin plastic film as a dielectric. They are widely used in power electronics due to their high accuracy, stability, and ability to handle high frequencies. They have a relatively long lifespan compared to electrolytic and ceramic capacitors and are less sensitive to temperature and voltage variations. However, they are relatively larger in size and more expensive than other capacitor types. Film capacitors are commonly used in high-frequency applications, such as switch-mode power supplies, resonant circuits, and frequency converters. [40][41]

Detail comparison is given in table 1.1. Where are compared capacitors voltage levels, capacitances, physical volume, lifespan, price and tolerance. It should be noted that in table 1.1 given values are averages, and mostly formed according to real existed large-scale manufactured capacitors. Values could differ in case of specific devices that are

Table 1.1

	Aluminium Electrolytic	Tantalum	Ceramic	Film
Voltage levels	Typically, up to 600V	Typically, up to 100V	Typically, up to 10kV	Typically, up to 10kV
Capacitance	1 μ F...1mF	1 μ F...1mF	1 μ F...500 μ F	1 μ F...400 μ F
Lifespan	Up to 5,000h	Up to 10,000h	Up to 10,000h	Up to 100,000h
Price	Low	High	Low	Medium
Tolerance	Low	High	Low	High
Volume	Large	Very Low	Low	Medium

As we can see from the table 1.1, every capacitor type has its advantages and disadvantages, and each type has his own niche where it is more suitable. When we are talking about applying as a filter in inverters, we must note that:

- 1 Lifespan must be high enough to ensure proper work during the lifespan of inverter itself. Nowadays the inverter lifespan can vary from 10 years to 15 which makes it up to 131,000 working hours.
- 2 Capacitor voltage level must be suitable.
- 3 Capacitor capacitance must be suitable.
- 4 The physical volume of the system must be as low as possible because it increases the effectiveness of the system. This parameter is more crucial when working with microinverters where the physical room is limited.

2. SELECTED MICROINVERTER TOPOLOGY

As it was described in the introduction part, the main goal of this thesis work is to apply active decoupling technique to a standard microinverter topology. This will help to increase power density of microinverter and make device more robust in case of working at high temperatures.

This is the practical part of thesis work and it consist of next parts:

- Review of proposed topology
- Calculation of components for proposed topology
- Calculation of power density

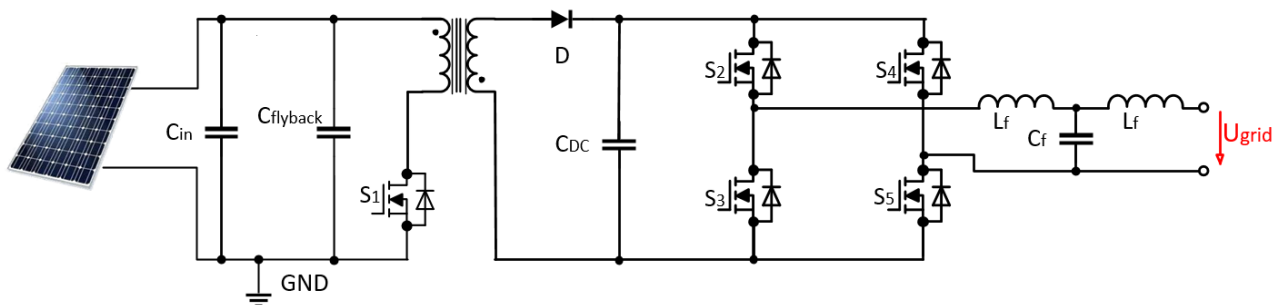


Figure 2.1 Proposed microinverter topology [33]

In this work, a flyback microinverter topology is used as a base for applying the active power decoupling topology. Flyback topology provides an opportunity to work in both ranges: buck and boost, depending on transformer windings ratio.

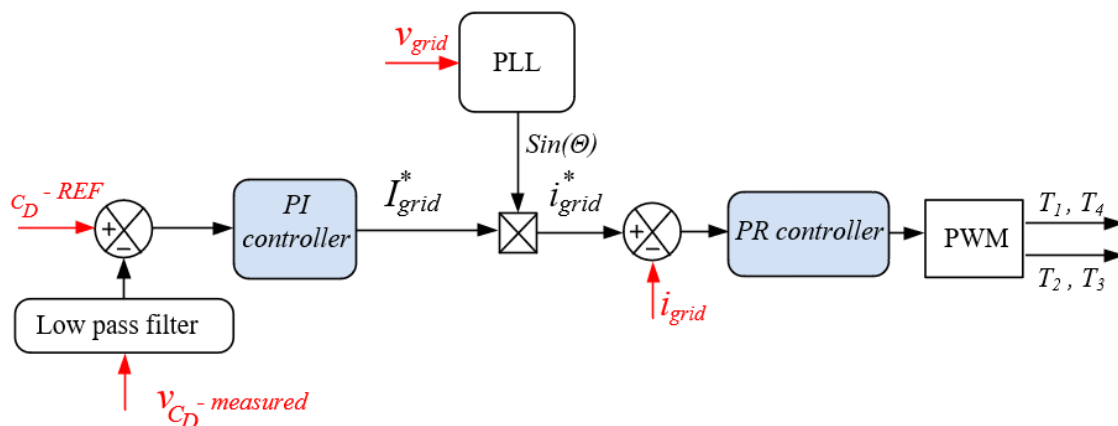


Figure 2.2 Control strategy for selected microinverter topology [33]

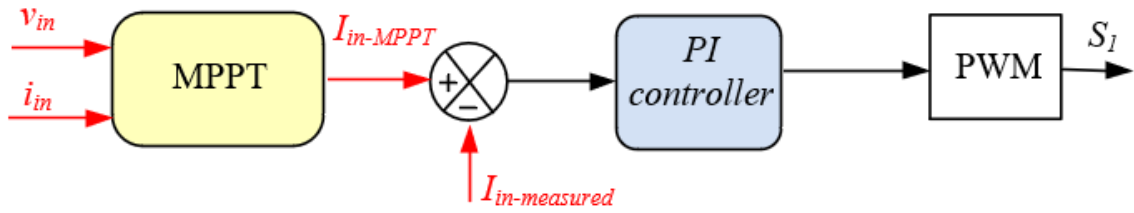


Figure 2.3 Control strategy for MPPT control.

In case of proposed flyback topology, the passive decoupling capacitor value can be calculated using next equation:

$$C_{DC} \geq \frac{P_{PV}}{\omega * U_{DC} * \Delta U_r} \quad (2.1)$$

where $\Delta U_r < 0.05$ – maximal allowable voltage ripple across capacitor,

U_{DC} – voltage across capacitor.

$$C_{DC} \geq \frac{426.3}{2\pi * 50 * 350 * 17.5} = 222\mu F$$

According to calculations, a 400V 250 μ F capacitor is chosen.

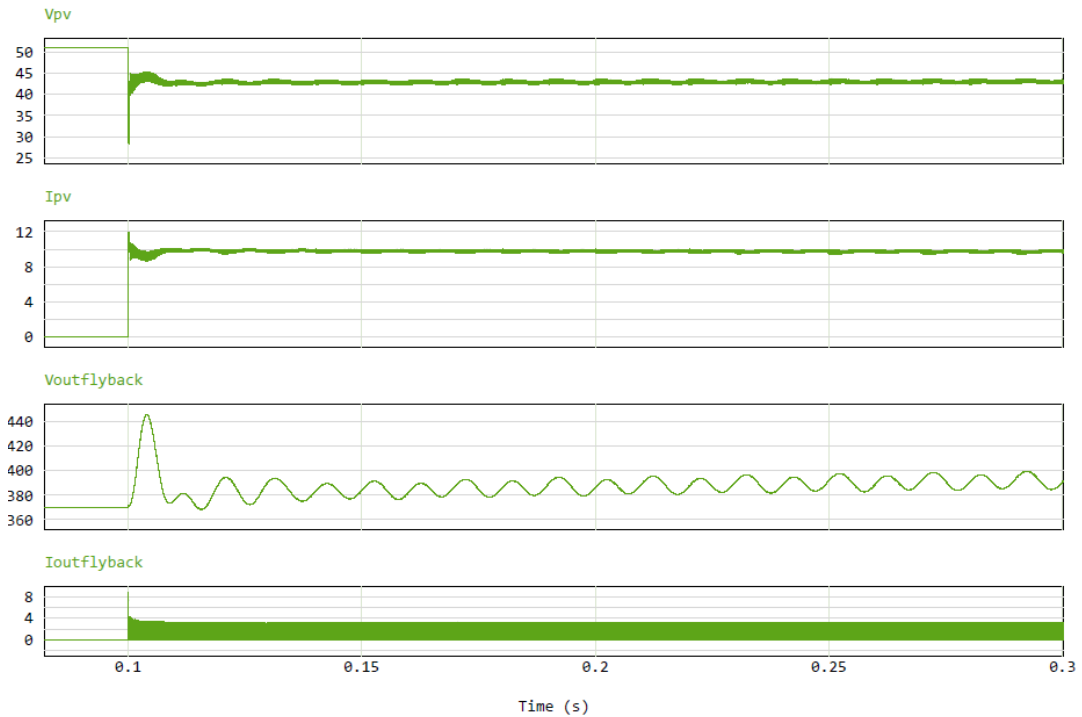


Figure 2.4 PV side and DC stage of inverter voltage and current values

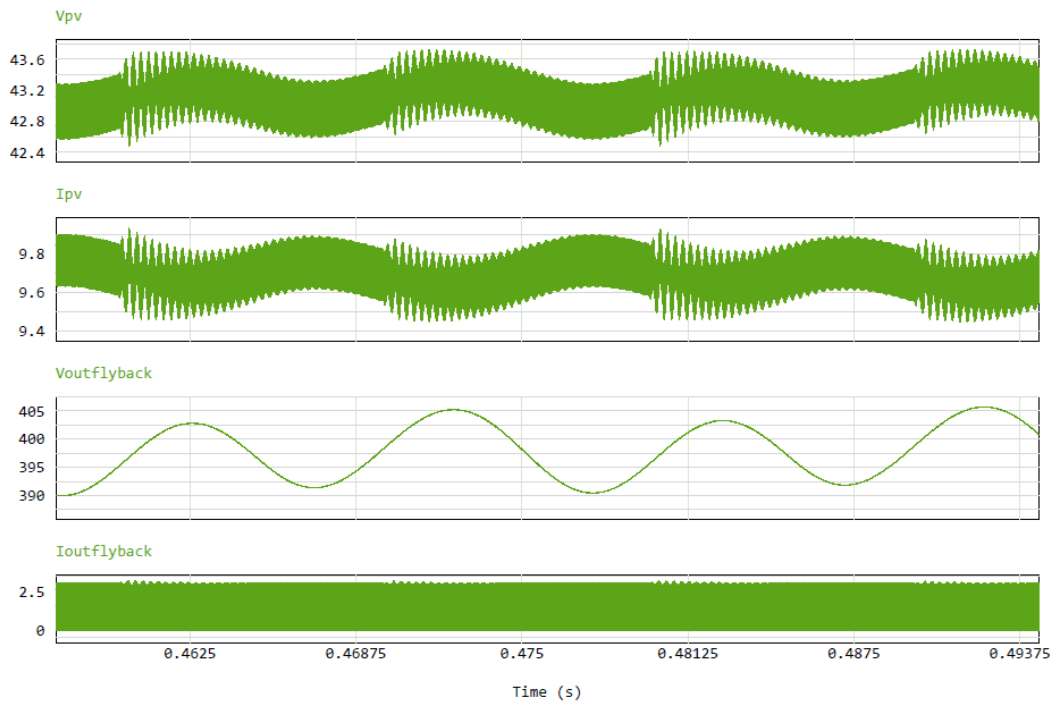


Figure 2.5 PV side and DC stage of inverter voltage and current values

As we can see from the figures 2.4 and 2.5, both – voltage and current ripple values with $C_{DC} = 250\mu F$ are within 5% of nominal. Voltage probe after flyback microinverter seems to be unstable until 0.5s of test time, it slightly increases during the whole test time and doesn't reach steady state.

2.1 Active power decoupling circuit and parameters calculation

Buck topology (Fig.1) is chosen as active power decoupling circuit. Buck topology is easiest topology to control and calculate. In case of Buck active ripple eliminator, the voltage across buffer capacitor should be smaller than voltage generated by PV panel.

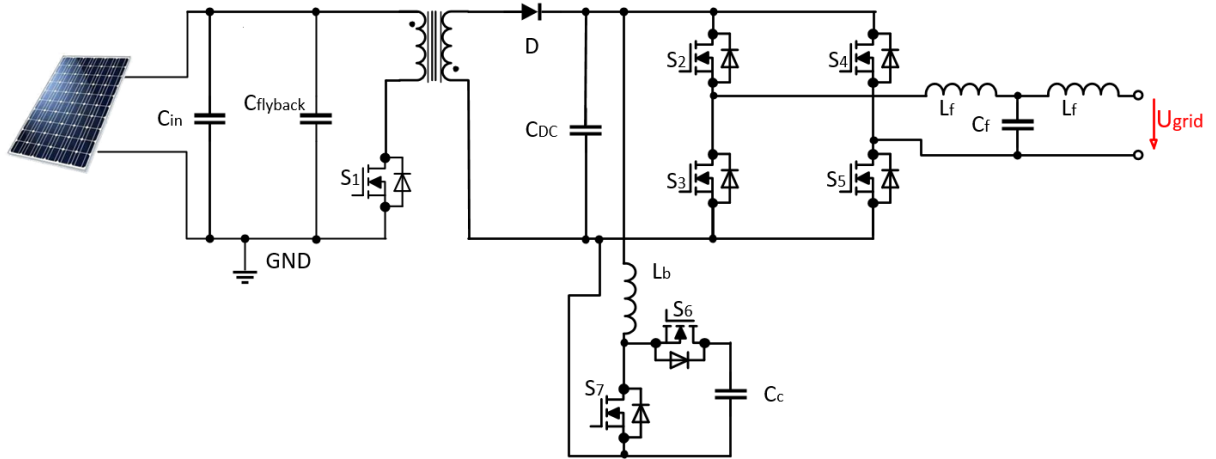


Figure 2.6 Selected microinverter topology with integrated active decoupling circuit

Table 2.1. Parameters of proposed system

PV maximal output voltage, V	U_{PV}	40.6
PV maximal output current, A	I_{PV}	10.5
PV maximal output power, W	P_{PV}	426.3
Grid frequency, Hz	f	50
Maximal allowed voltage ripple, % of nominal	ΔU_r	5
Maximal allowed current ripple, % of nominal	ΔI_r	5
Voltage across APD capacitor, V	U_c	>350
APD MOSFETs switching frequency, Hz	f_{SW}	60000
DC-link voltage, V	U_{DC}	350

In case of active power decoupling, the buffer capacitor value is oriented to be dealing mainly with second harmonic component, so the system parameters are significantly lower than in case of passive decoupling. It must be noted that this method is suitable for decreasing physical volume of the system but is not suitable for completely refusing of using passive filter. Passive filter is still needed to compensate high frequency components of the system, but when passive filter is used together with active one, both circuits can be more precisely designed and as a result – lower physical volume will be achieved.

Decoupling capacitor capacitance can be calculated using following equation [30]:

$$C_C = \frac{(K + 1) * P_{PV}}{\omega U_C^2}, \quad K \geq 1 \quad (2.2)$$

$$C_C = \frac{2 * 426.3}{2\pi * 50 * 700} = 7.54 * 10^{-6} = 7.54\mu F$$

If current second harmonic is now filtered by using active power decoupling circuit, it means that DC-link capacitor value can now be decreased because it doesn't have to manage with lower harmonic and can be designed to filter high-frequency components.

DC-link capacitor minimal value can be calculated using next equation [35]:

$$C_{DC} = \frac{I_{DC} * T_{SW}}{2 * \Delta U_{r,DC} * U_{DC}} \quad (2.3)$$

where I_{DC} – amplitude of current across DC-link capacitor,

T_{SW} – switching period,

$\Delta U_{r,DC}$ – allowable voltage ripple across DC-link capacitor.

Thus, minimal suitable capacitance is:

$$C_{DC} = \frac{1.218 * 1.67}{2 * 0.05 * 350} = 0.00000058F = 0.58\mu F$$

2.1.1 Active power decoupling circuit working mode

Two types of working modes were compared in case of proposed active power decoupling circuit: Continuous Conduction Mode (CCM) and Discontinuous Conduction Mode (DCM). Detailed comparison of those working modes is described below:

- Operating region: In CCM, the inductor current never reaches zero during one switching cycle, while in DCM, the inductor current drops to zero at some point during the cycle.
- Output ripple: CCM generally has lower output ripple than DCM due to the continuous current flow through the inductor.
- Efficiency: The efficiency of the converter in CCM is generally higher than in DCM, especially at high load currents. This is because in CCM, the inductor current is always flowing, which reduces switching losses.

- Design complexity: CCM designs can be more complex than DCM designs due to the need to maintain continuous inductor current.
- Component selection: The choice of inductor and capacitor values can be different between CCM and DCM. In CCM, the inductor value is generally higher than in DCM due to the continuous current flow.
- Noise: DCM can produce more audible noise due to the large voltage and current spikes that occur during the switching cycle.

To sum up, Discontinuous Conduction Mode is more suitable when easier control technique and smaller size of system is needed, while Continuous Conduction Mode is a good choice when high efficiency and low noise factor is crucial factor.

As the main aim of this thesis work is to make microinverter with maximal power density and easier control algorithm, the DCM working mode was chosen.

To make sure active power decoupling circuit is working in Discontinuous Conduction Mode, an auxiliary inductance should be correctly calculated. For working in DCM mode, the auxiliary inductance must be full charged and discharged during each switching period.

$$T_{SW} < t_1 + t_2 \quad (2.3)$$

where T_{SW} – switching period,

t_1 – charging period,

t_2 – discharging period.

Switching period can be obtained using following equation:

$$T_{SW} = \frac{1}{f_{SW}} \quad (2.4)$$

To satisfy this requirement, the maximal auxiliary inductance can be calculated as follows:

$$L_{MAX} \leq \frac{T_{SW}}{2 * i_c} * \frac{U_{DC} * U_C - U_C^2}{U_{DC}} \quad (2.5)$$

where i_c – average current across inductor

$$i_c = \frac{P_{PV} * \sin(2\omega t)}{\sqrt{\frac{P_{PV}}{C_c * \omega}} * (K - \cos(2\omega t))} \quad (2.6)$$

where K – energy storage margin coefficient, $K \geq 1$. If coefficient is 1, it means that auxiliary capacitor is fully charged and discharged during one switching period.

The second parameter to define auxiliary inductance is its ability to work with maximal current. In this case minimal inductance suitable for working at maximal currents can be calculated using next equation:

$$L_{MIN} \geq \frac{2 * T_{SW} * i_c}{I_{PV}^2} * \frac{U_{DC} * U_C - U_C^2}{U_{DC}} \quad (2.7)$$

According to (2.3) and (2.5) a buffer inductor inductance must be:

$$\frac{2 * T_{SW} * i_c}{I_{PV}^2} * \frac{U_{DC} * U_C - U_C^2}{U_{DC}} \leq L_d \leq \frac{T_{SW}}{2 * i_c} * \frac{U_{DC} * U_C - U_C^2}{U_{DC}} \quad (2.8)$$

Calculations for buffer inductor inductance were made using Microsoft Excel software for one switching period with a step of $0.025T_S$. As a result of calculations, the buffer inductor must be chosen between next interval:

$$97 \mu H \leq L_b \leq 1140 \mu H$$

2.1.2 Active power decoupling circuit

In this thesis work, a boost type active decoupling circuit was chosen due to easier control technique required to compensate power ripples. The boost circuit working principle is to compensate ripple power by injecting an equal but inversed power. In this case the boost circuit is working as a current source.

The proposed compensation principle is based on compensation of current waveforms that are different than average value. Compensation value is found using next equation.

$$i_{comp} = i_{full} - i_{mean} \quad (2.9)$$

where i_{comp} – compensated current,

i_{full} – full current,

i_{mean} – average current.

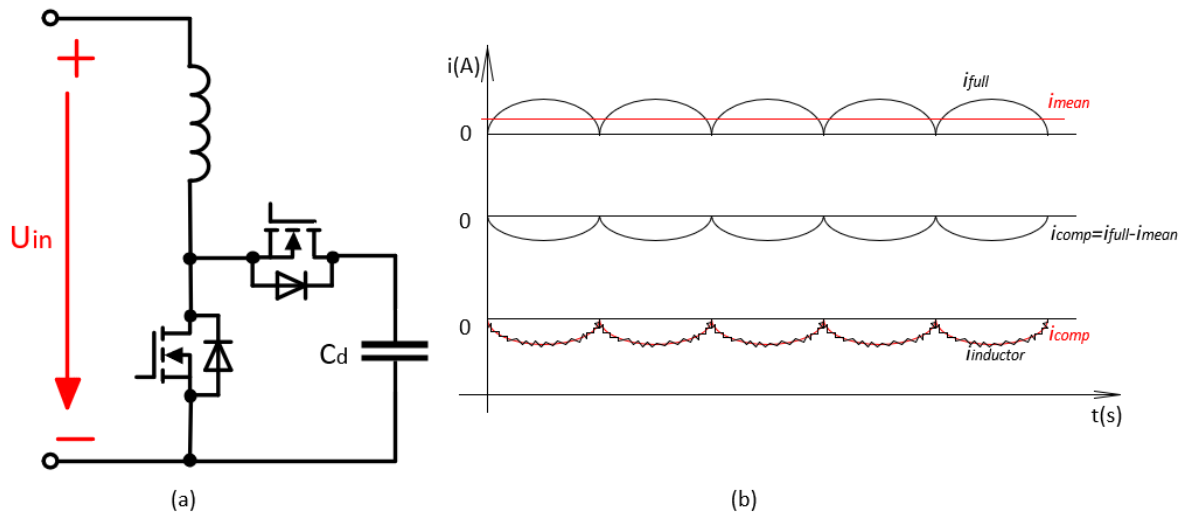


Figure 2.7 (a) – proposed active power decoupling circuit, (b) – current values of working active decoupling circuit

Hysteresis control is proposed as a control technique for active power decoupling circuit. Hysteresis control is based on a reference value that is calculated according to equation 2.7. By switching switches 1 and 2, compensated current value is made to be closer to reference value.

3.CONTROL STRATEGY

3.1 Fast Fourier Transform

Fast Fourier Transform (FFT) is a widely used algorithm in signal processing that efficiently computes the Discrete Fourier Transform (DFT) of a sequence of numbers. The FFT algorithm is widely used in the field of power electronics to analyze spectral composition of signal.

The Fourier Transform is a mathematical technique that converts a time-domain signal into a frequency-domain signal. It is used to identify the frequency components of a signal, which can be used for various purposes such as filtering, noise reduction, and feature extraction. However, the Fourier Transform has a high computational complexity, which makes it impractical for processing large data sets in real-time applications. [44][45]

FFT is an efficient algorithm for computing the DFT, which significantly reduces the computational complexity of the Fourier Transform. This improvement in the computational complexity of the FFT algorithm has made it possible to process large data sets in real-time applications. [44][45]

The FFT algorithm breaks down the DFT computation into smaller sub-problems, each of which can be solved independently. The sub-problems are then combined to obtain the result of the DFT. This process of breaking down the computation into smaller subproblems is called the divide-and-conquer strategy.[45]

The FFT algorithm is implemented using various techniques such as the Cooley-Tukey algorithm, Radix-2 algorithm, and the Bluestein algorithm. The Cooley-Tukey algorithm is the most widely used technique for implementing the FFT algorithm, and it is based on the Radix-2 algorithm. [43]

The FFT algorithm is a powerful tool for processing signals in various applications. Its efficient nature has made it possible to process large data sets in real-time applications. The Cooley-Tukey algorithm is the most widely used technique for implementing the FFT algorithm, and it is based on the Radix-2 algorithm. [43]

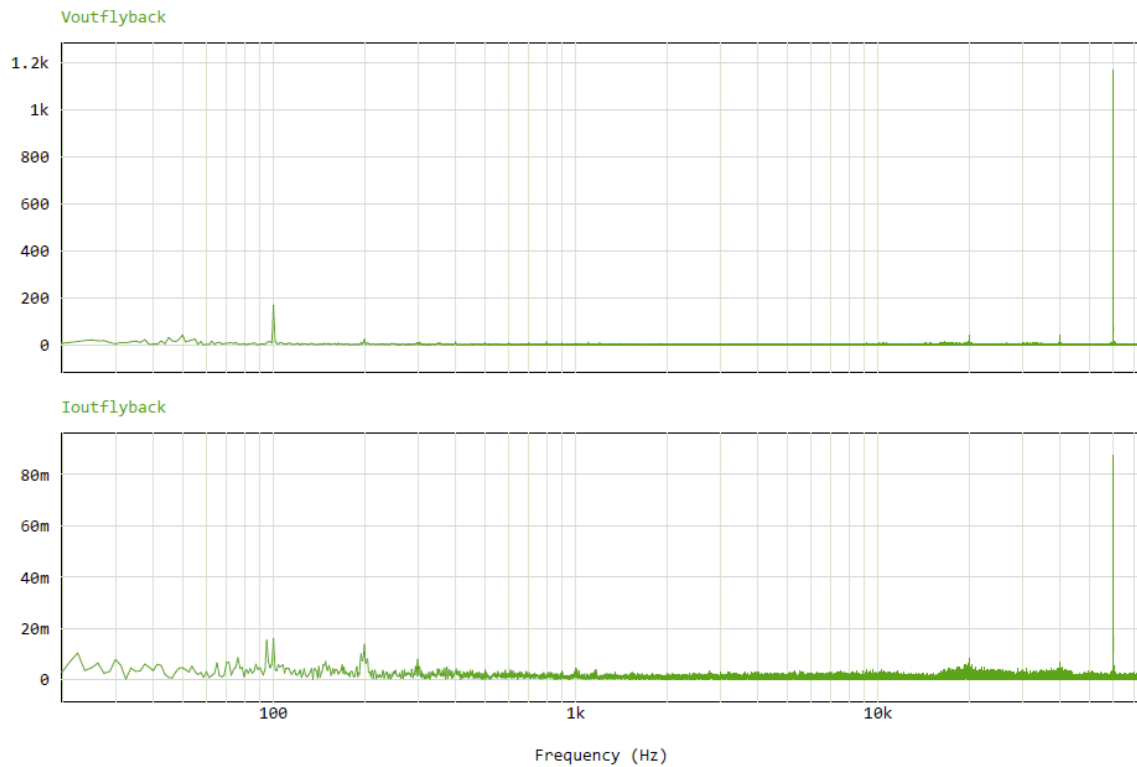


Figure 3.1 Spectral analysis of DC stage voltage and current parameters

From Fig. 3.1 we can see a graph that was configured in PSIM software and shows us a spectral analysis of voltage and current components on the secondary site of flyback converter. Spectral analysis shows us that voltage component main disturbance appears at 100 Hz frequency.

3.2 Proposed control strategy

As it was mentioned before, the proposed control strategy is based on hysteresis control principle. In this case, the reference current can be calculated using standard mathematical equations or measured using some sophisticated devices.

In this thesis work, obtaining the reference value were examined in two ways:

- Calculated from grid site pure sinusoidal signal using mathematical equations:

$$I_{mean} = \frac{2\sqrt{2}}{\pi} * I_{RMS} \quad (3.1)$$

This method was used because of peculiarity of PSIM software to not to calculate mean value from raw signal. Method is not so precise because it can work only in ideal conditions. As a result of its drawback, this method was only used in

educational reason – active power decoupling circuit was tuned to working condition using this reference current value.

- Captured using average voltage sensor on DC site. With this method, reference current value contains also current ripples.

3.2.1 Proposed control scheme

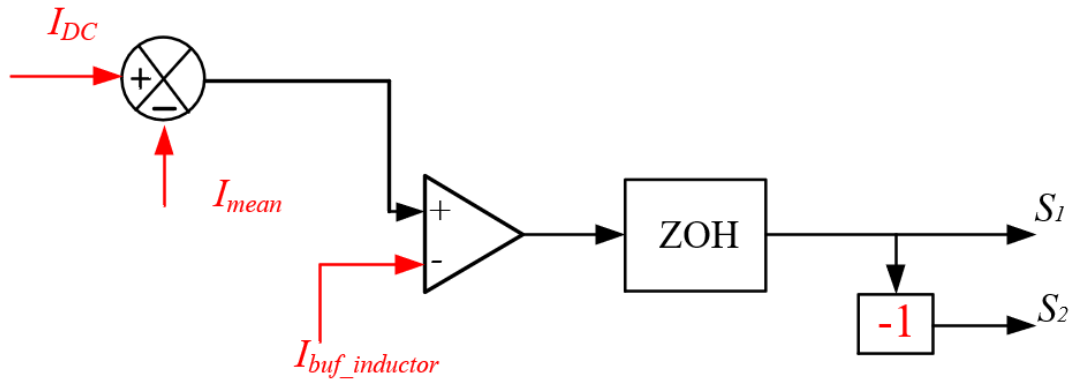


Figure 3.2 Proposed control method.

As it is shown on picture above, the Zero-Order Hold (ZOH) filter is used to generate signal values for active decoupling circuit switches. The ZOH filter is used to convert a continuous-time signal into a discrete-time signal, which can be processed by a digital controller.

The ZOH filter works by holding the input signal value constant for a fixed period of time, which is called the sampling time – in case of this control scheme, sampling frequency is fixed to 60kHz (sampling time is $1.67 \cdot 10^{-5}$). The sampling time determines the rate at which the input signal is sampled and converted into a discrete-time signal. The ZOH filter approximates the continuous-time signal by holding the input signal value constant for the duration of the sampling time. The output of the ZOH filter is a staircase-like waveform, where the height of each step corresponds to the input signal value during the sampling time.

3.3 Control strategy 2

In this section is shown alternative filtering method which is based on eliminating second order ripples. This method was introduced and used in [31] and [32] and oriented to buck-boost type ripple eliminator circuit. In this thesis work given algorithm is adopted and changed for working with boost-type circuit.

Duty cycle calculation, control and implementation is used by estimation and control of inductor current change during switching period of auxiliary circuit switches.

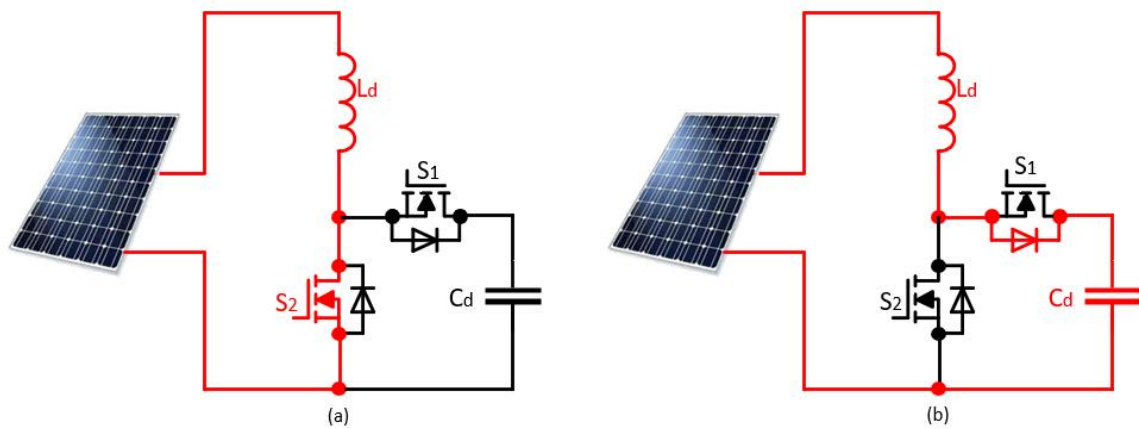


Figure 3.3 Circuit working mode during charging period, (a) – S2 is ON, (b) – S1 and S2 are OFF.

Figure 3.3 shows us how change working modes of decoupling circuit during charging period ((a) – during DT, (b) – during D'T) During capacitor charging period its current change can be estimated and calculated according to the next graph:

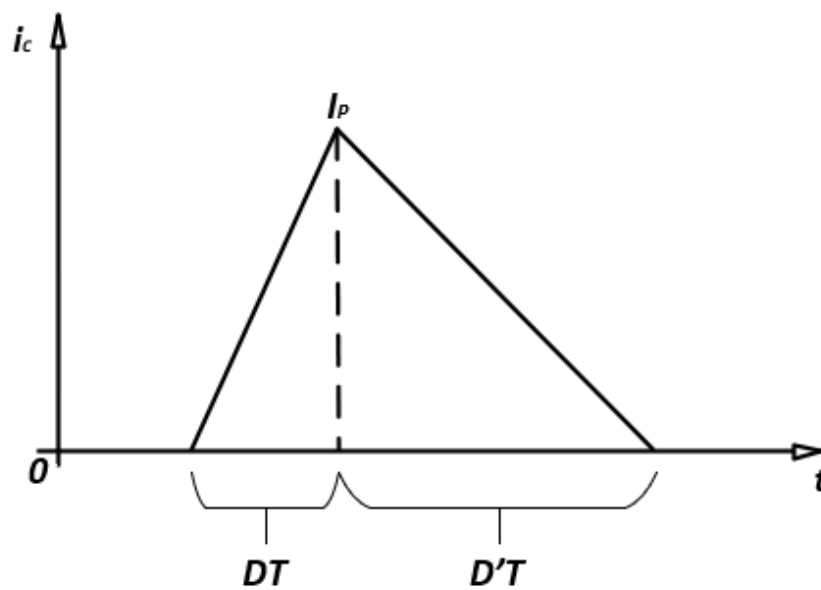


Figure 3.4 Graph of inductor current during charging period.

If we put together both: Fig. 3.3 and Fig. 3.4, we can easily calculate duty cycles knowing how changes the inductor current during cycles DT (S2 ON) and D'T (S1 and S2 OFF). For calculating duty cycles a simple geometry is used:

$$\begin{cases} i_{cavg}T = \frac{1}{2} * I_p * (D + D')T \\ I_p = \frac{U_{DC}}{L_b} * DT \\ I_p = \frac{U_{DC} - U_C}{L_d} * D'T \end{cases} \quad (3.1)$$

where i_{cavg} – average current across inductor,

I_p – peak current across inductor.

From Eq. 3.1 we can obtain the duty cycle value by comparing both maximal inductor values:

$$\frac{U_{DC}}{L_d} * DT = \frac{U_{DC} - U_C}{L_d} * D'T \rightarrow D' = \frac{U_{DC}}{U_{DC} - U_C} D \quad (3.2)$$

By replacing I_p and D' in first part of (Eq. 3.1) with their values, we get an equation that can be simplified to:

$$i_{cavg} = \frac{1}{2} * \frac{U_{DC}}{L_d} DT * \left(D + \frac{U_{DC}}{U_{DC} - U_C} D \right) \rightarrow D = \sqrt{\frac{2i_{cavg}L_d(U_C - U_{DC})}{U_{DC} * U_C * T}} \quad (3.3)$$

Calculation of duty cycle for switch S1 is shown below and it is based on same algorithm but applied for inductor current change during discharging period.

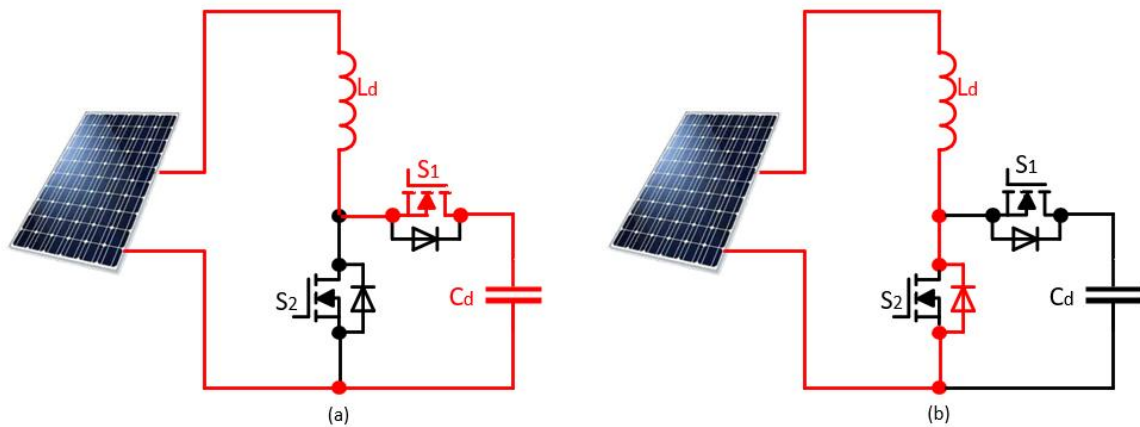


Figure 3.5 Circuit working mode during inductor discharging period, (a) – S1 is ON, (b) – S1 and S2 are OFF.

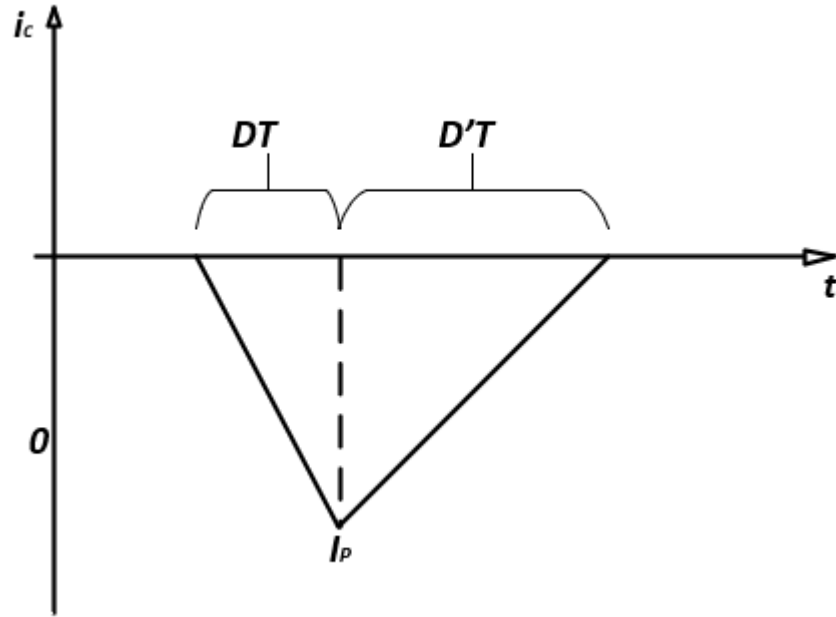


Figure 3.6 Graph of inductor current during discharging period.

Calculation of duty cycle for switch S1:

$$\left\{ \begin{array}{l} i_{cavg}T = \frac{1}{2} * I_p * (D + D')T \\ I_p = \frac{U_C - U_{DC}}{L_d} DT \\ I_p = \frac{U_{DC}}{L_d} D'T \end{array} \right. \quad (3.4)$$

D' can be derived as follows:

$$D' = \frac{U_C - U_{DC}}{U_{DC}} D \quad (3.5)$$

Using Eq. 3.3 and Eq. 3.4 calculation of duty cycle is shown below:

$$i_{cavg} = \frac{1}{2} * \frac{U_C - U_{DC}}{L_d} DT * \left(D + \frac{U_C - U_{DC}}{U_{DC}} D \right) \rightarrow D = \sqrt{\frac{2i_{cavg}L_dU_{DC}}{(U_C - U_{DC})U_C T}} \quad (3.6)$$

3.3.1 Control scheme

To make control circuit work for elimination second order ripples the current before active power decoupling circuit must be measured and its second harmonic should be filtered. Second harmonic of current parameter could be obtained using resonant filter [31][32]:

$$K_R(s) = \frac{2\xi h\omega s}{s^2 + 2\xi h\omega s + (h\omega)^2} \quad (3.7)$$

where $h = 2$, in case of second harmonic,

$\xi = 0.01 - 0.02$ – damping ratio of the filter.

In this thesis work the second harmonic is filtered using standard Band-Pass filter block with following transfer function:

$$G(s) = \frac{Bs}{s^2 + Bs + \omega_0^2} \quad (3.8)$$

where $B = f_b * 2\pi$, and f_b is frequency width of the passing band,

$\omega_0 = f_0 * 2\pi$, and f_0 is center frequency of the filter.

Voltage control of buffer capacitor is done using next algorithm:

1. Voltage across capacitor is measured.
2. DC component of voltage value is extracted using filter.
3. DC component is compared to reference value, giving an error value as a result.
4. Error value is sent to PI controller. Output of PI controller is a current needed to charge buffer capacitor.

In [31][32] a first order hold filter is proposed to obtain the voltage DC component. Hold filter transfer function is shown below:

$$H(s) = \frac{1 - e^{-\frac{Ts}{2}}}{\frac{Ts}{2}} \quad (3.8)$$

In this thesis work, a voltage filter is done by using Low-Pass filter block in PSIM software. Additionally, a DC component could be obtained using an average voltage sensor when comparing a full wave voltage to average voltage value.

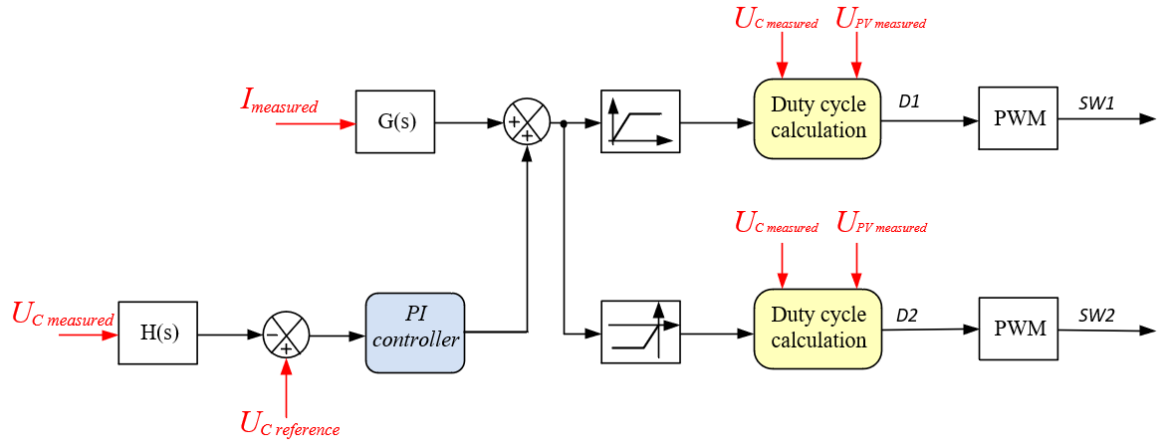


Figure 3.7 Active decoupling circuit control scheme.

To sum up, this control scheme is based on compensating DC current second harmonic component. Second harmonic is obtained by using Band-Pass filter on the DC current values. Filtered 2nd harmonic of current value is added to value, generated by PI controller and needed to control capacitor voltage. Then, depending on the sign of compensation current, a different duty cycle calculations are made, and different switching are in action. As there is made a control of current sign, both switches cannot be in action simultaneously.

3.4 Control strategy 3

Reviewed in this section control strategy is based on [34]. This method is also based on compensation of second harmonics. Feed forward control technique is used to control active power decoupling circuit current. Feed forward reference current can be calculated using next equation [34]:

$$i_{comp} = \frac{P_{comp}}{U_{DC}} * \cos 2\omega t \quad (3.9)$$

where P_{comp} – compensation power.

Control algorithm is based on compensating ripple power, so it is oriented to be smaller than in case of passive decoupling. Algorithm is also based on compensation of second harmonic using active circuit. This type of compensation allows us to significantly decrease a DC-link capacitor value, because it can be focused only on filtering high-frequency components.

One of the key advantages of feed forward current control is that it can provide fast response times and high accuracy in current control. Another advantage is that feed forward control decreases a complexity of control scheme.

One of disadvantages is that tuning of feed forward control circuit can be more complicated than in case of other techniques. This can be a complex and time-consuming process, requiring a deep understanding of the system's behaviour and characteristics. Additionally, the feed forward loop may not be able to compensate for all the nonlinearities in the system, which can limit its effectiveness in some applications.

3.4.1 Control scheme

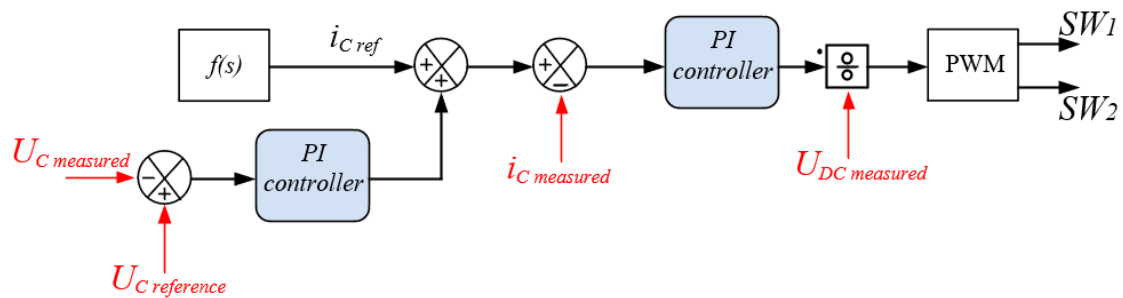


Figure 3.8 Active decoupling circuit control scheme.

Figure 21 shows us a control technique proposed in [34]. Inductor current reference value is found using Eq. (3.9) and adding calculated value to output of PI controller which is used to generate additional current value that is needed to keep voltage across capacitor at given value. After comparing reference current value to measured one, another PI controller generates needed output to keep real current at given value.

4. EXPERIMENTAL RESULTS AND SIMULATION VERIFICATION

In this topic we will review how does different control strategies perform and compare the results of simulations. Proposed control strategy will be compared to strategies that are proposed by other authors and adopted for using in proposed microinverter.

Using equations that were described earlier, range of passive elements parameters was calculated and using try and error method proper parameters were found. Next parameters were used in test simulation of decoupling circuit:

Table 4.1 Experimentally found values of components

	$L_d, \mu H$	$C_C, \mu F$	$C_{DC}, \mu F$
Proposed control	800	8	40
Control technique 2	800	60	40
Control technique 3	800	80	60

4.1 Experimental results of proposed control strategy

In this topic will be reviewed the results of simulation of proposed control strategy.

From Fig. 4.1 we can see how change values of DC link voltage and current when active decoupling circuit starts working. The voltage across DC link before activating decoupling circuit significantly exceeds the limit for voltage ripple ($\Delta U = 350 - 220 = 130V$). With the help of active decoupling circuit, DC link voltage level is now set to be inside the allowable range ($\Delta U = 410 - 385 = 25V$).

As seen from Fig. 4.2, the voltage level of active decoupling capacitor is relatively high and almost reaches 1kV. This may lead to increased volume of decoupling capacitor and as a result – to increased volume of whole system.

Unfortunately, proposed control does not provide a proper control of voltage across active decoupling capacitor. If voltage level could be decreased, capacitor physical size could be also decreased.

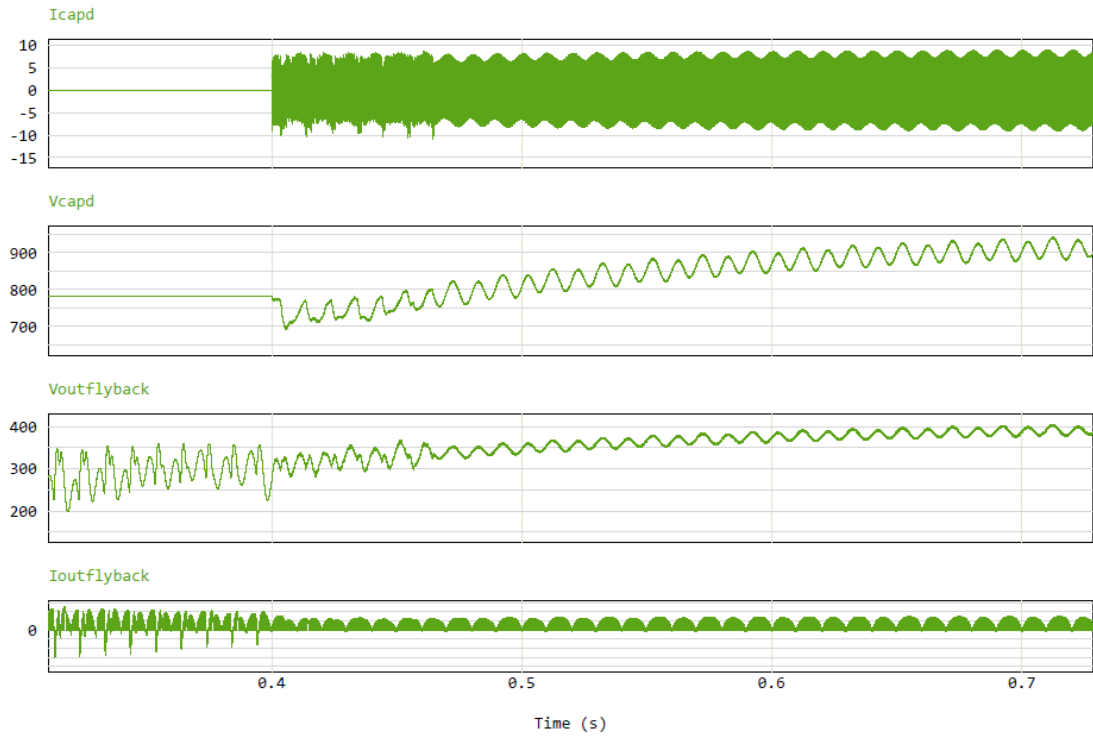


Figure 4.1 Active decoupling circuit and DC stage of inverter voltage and current values (proposed control)

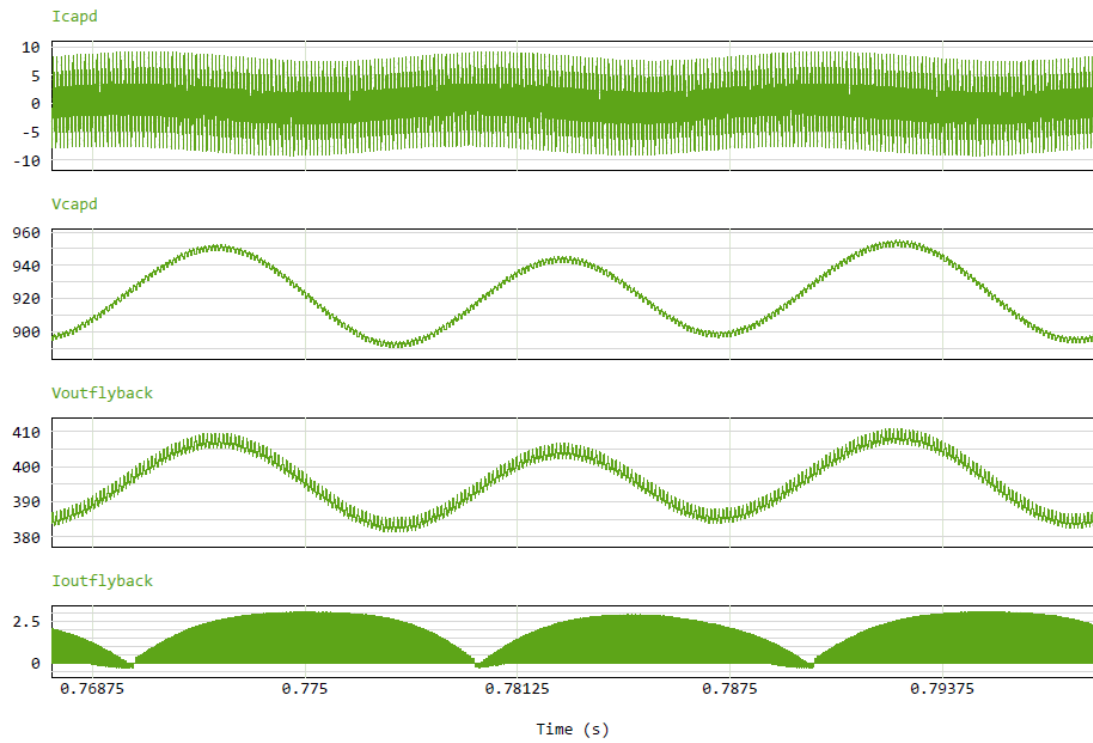


Figure 4.2 Active decoupling circuit and DC stage of inverter voltage and current values, zoomed (proposed control)

Meanwhile, Fig. 4.3 and 4.4 show us the difference in PV site current and voltage components when working without active circuit and with it. As seen, active filter works properly, and current and voltage levels are filtered enough to be suitable for proper working of the system.

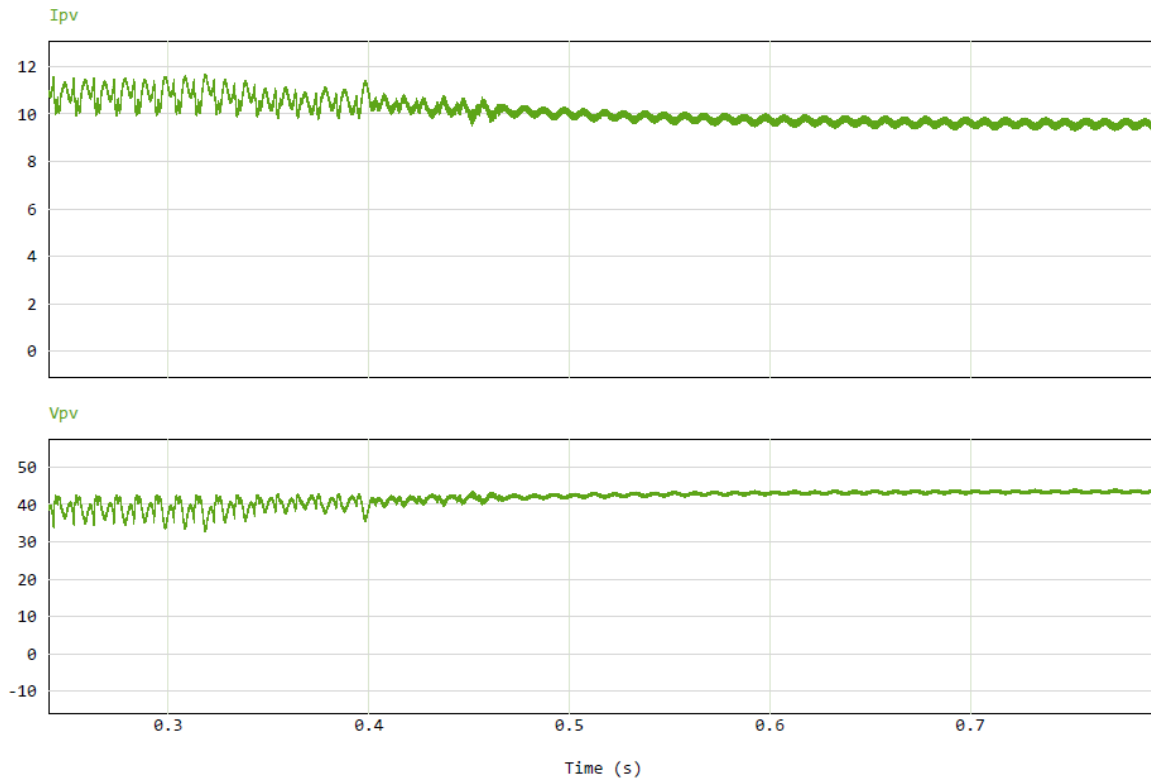


Figure 4.3 Voltage and current values on PV side (proposed control)

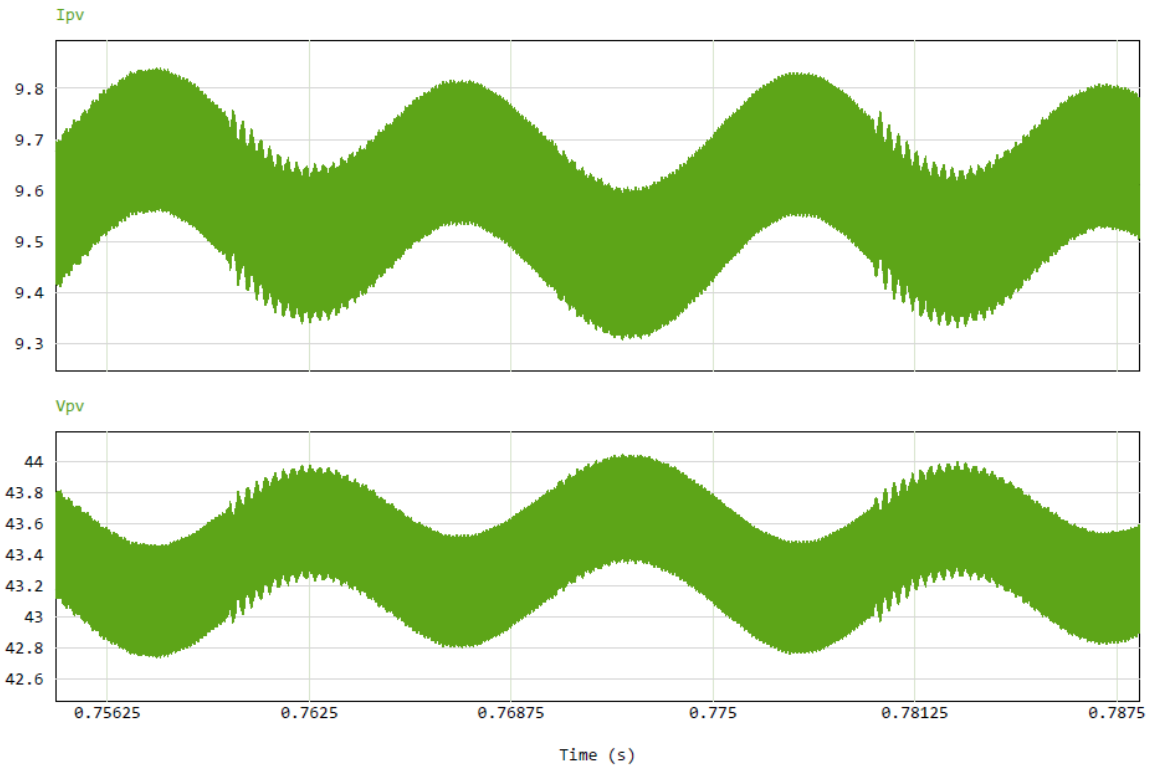


Figure 4.4 Voltage and current values on PV side, zoomed (proposed control)

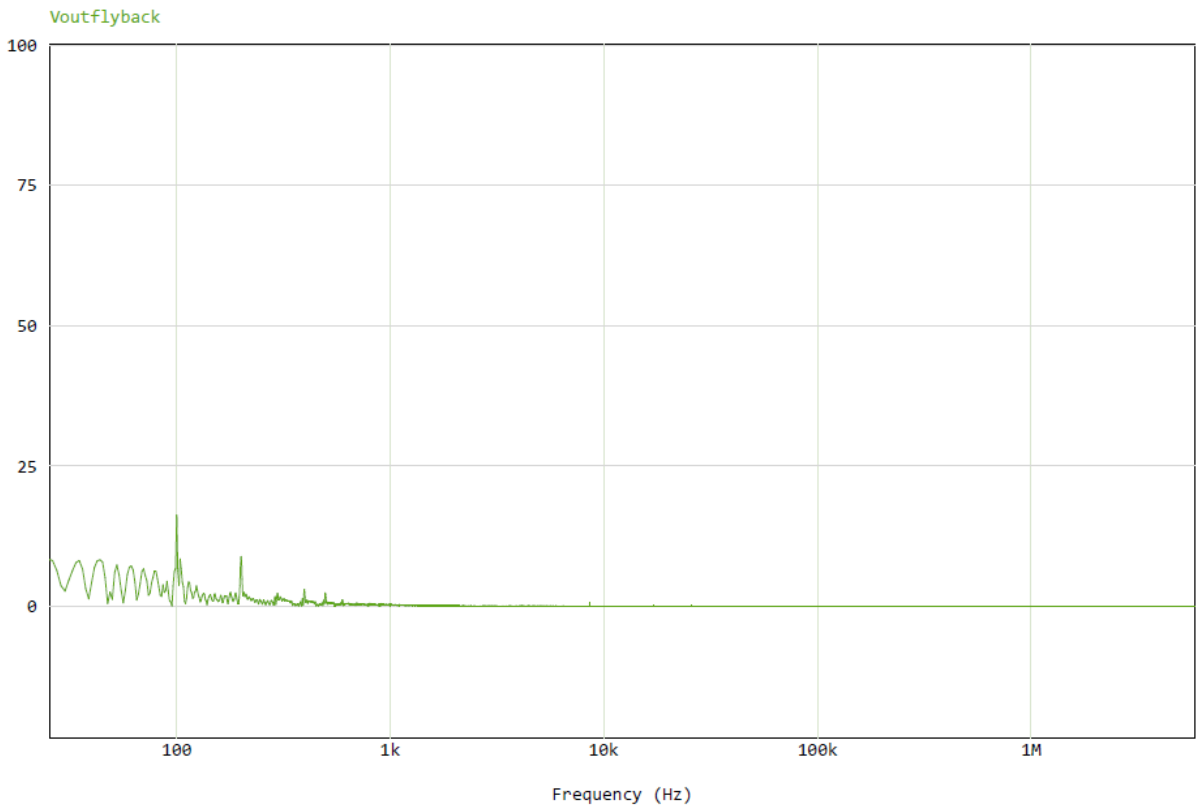


Figure 4.5 DC stage voltage spectral analysis (proposed control)

As a result of active decoupling, there is almost no second harmonic component in DC link voltage. The amplitude of 2nd harmonic is decreased 8 times to the level of 15 p.u.

Fig. 4.5 shows us that this hybrid decoupling circuit also successfully filters high-frequency components that appear because of main converter transistors switching frequency.

4.2 Experimental results of control strategy 2

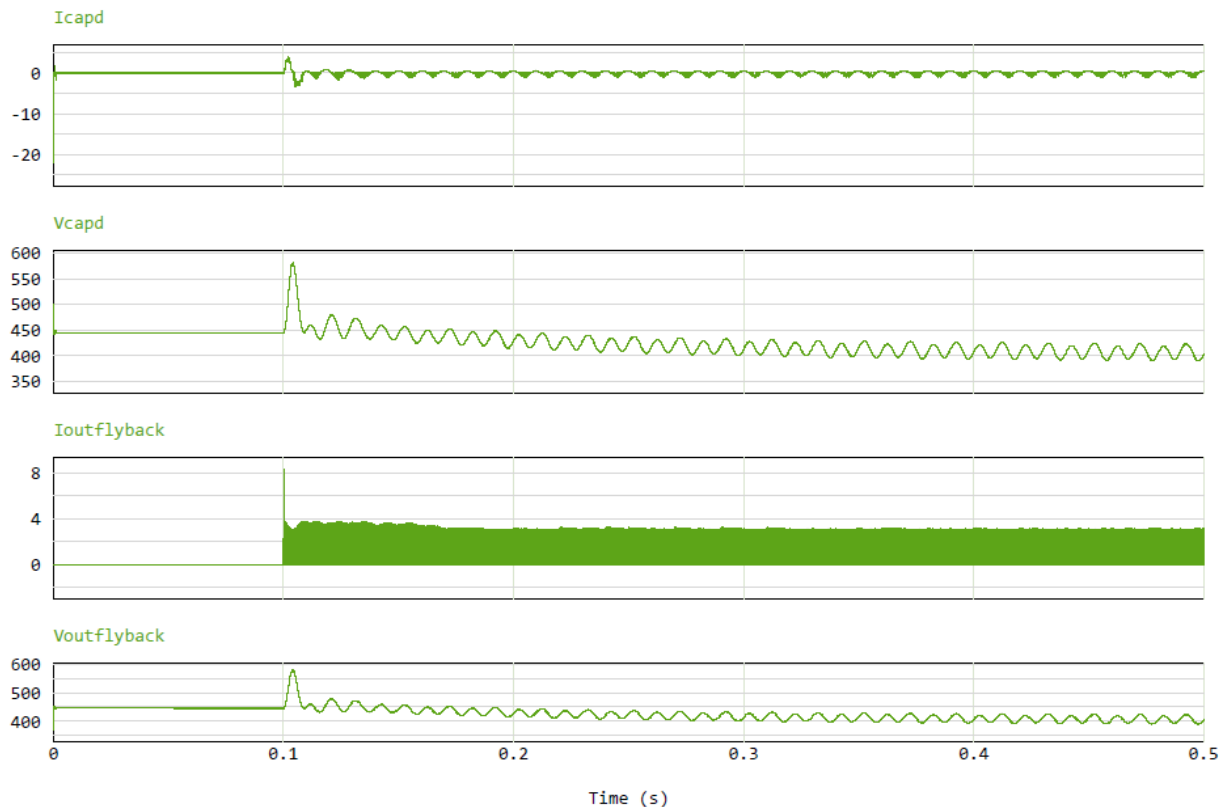


Figure 4.6 Active decoupling circuit and DC stage of inverter voltage and current values (control strategy 2)

Fig. 4.6 shows us voltage and current parameters across active decoupling capacitor and voltage and current parameters of DC stage of microinverter.

In case of active decoupling circuit, its reference voltage across capacitor is controlled to be 500V, but as it is seen from Fig. 4.6, its value reaches its steady state at value 400V.

Different from proposed control, DC link voltage at the start of working process is quite high and average voltage even reaches 450V. This component reaches steady state also at 0.5s of modulation period.

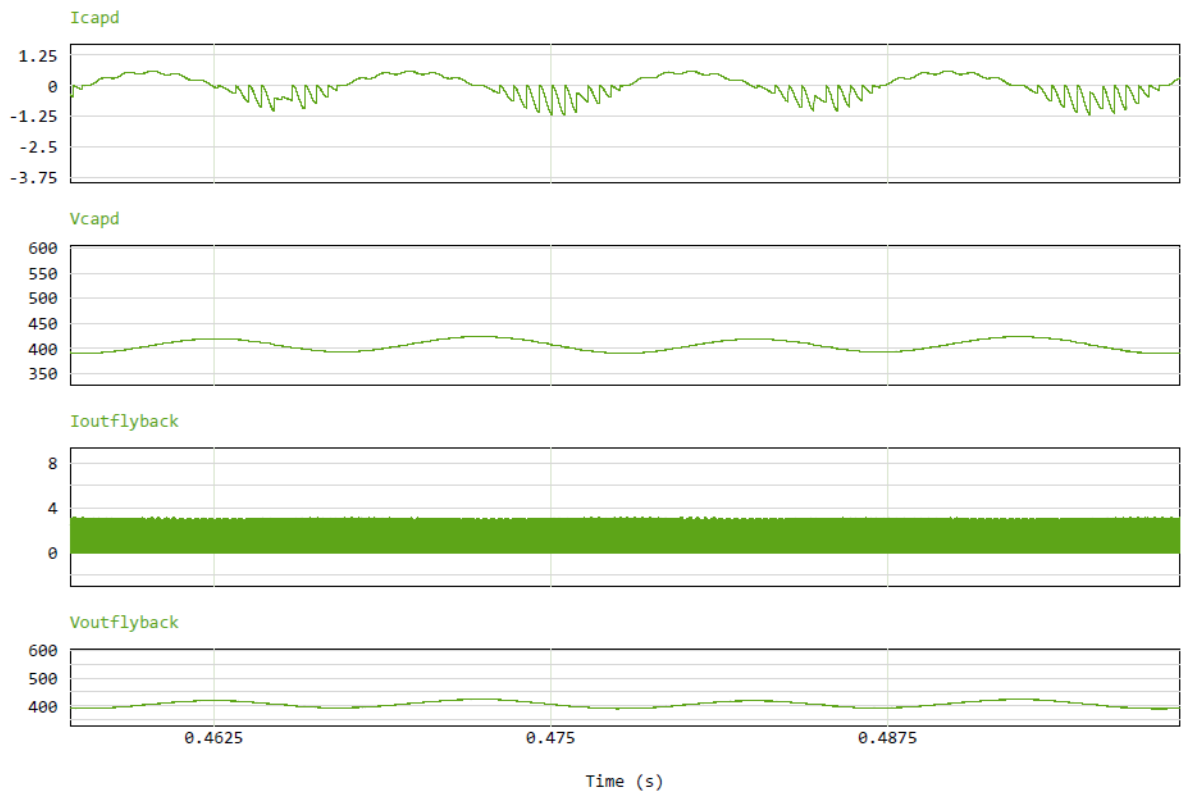


Figure 4.7 Active decoupling circuit and DC stage of inverter voltage and current values, zoomed

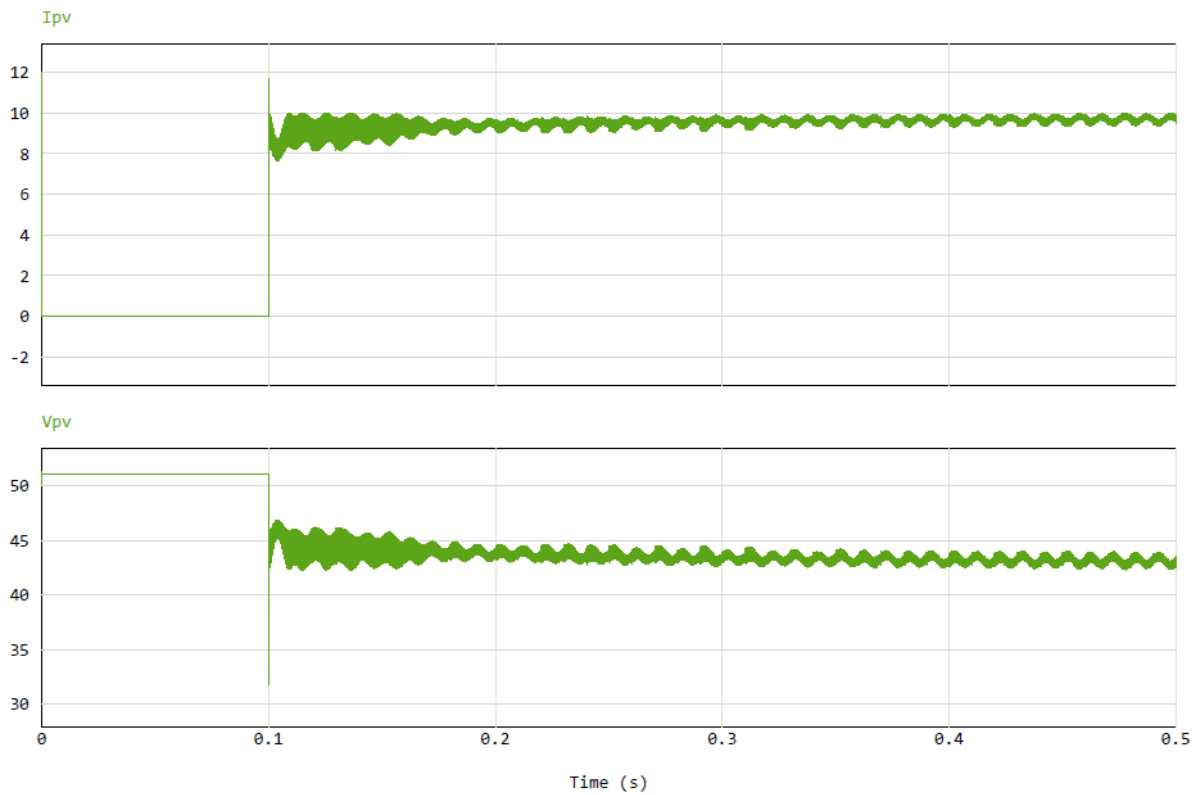


Figure 4.8 Voltage and current values on PV side (control strategy 2)

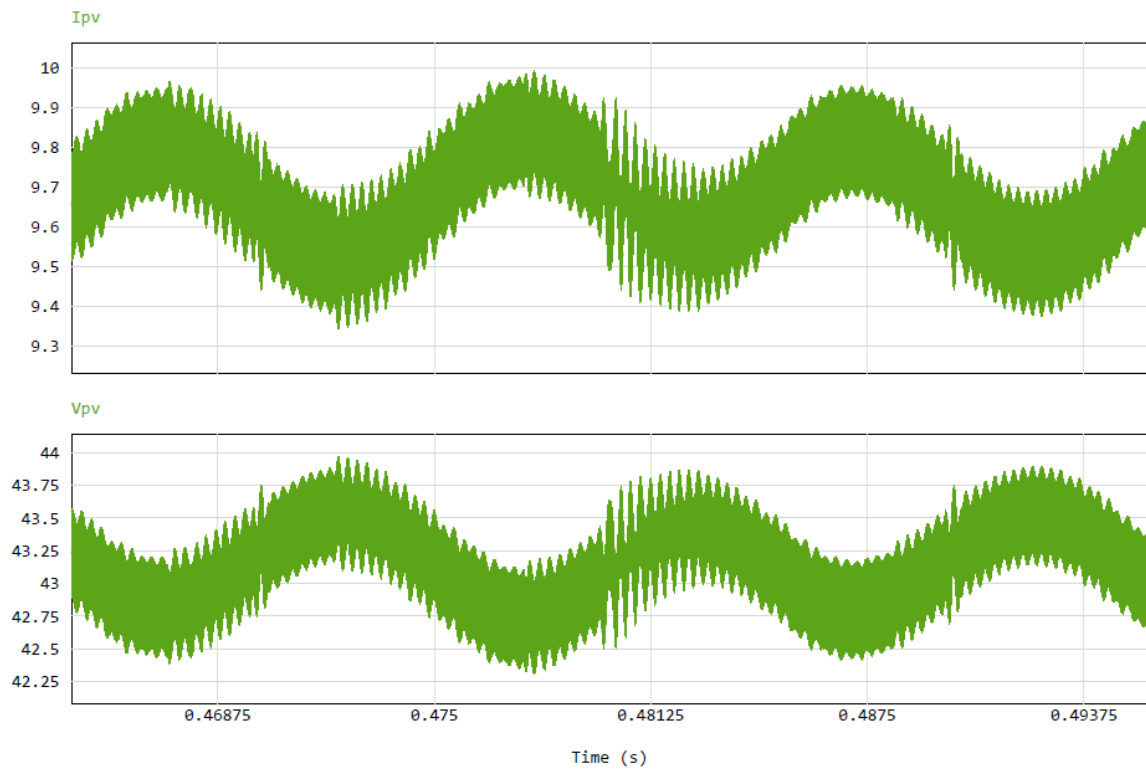


Figure 4.9 Voltage and current values on PV side, zoomed (control strategy 2)

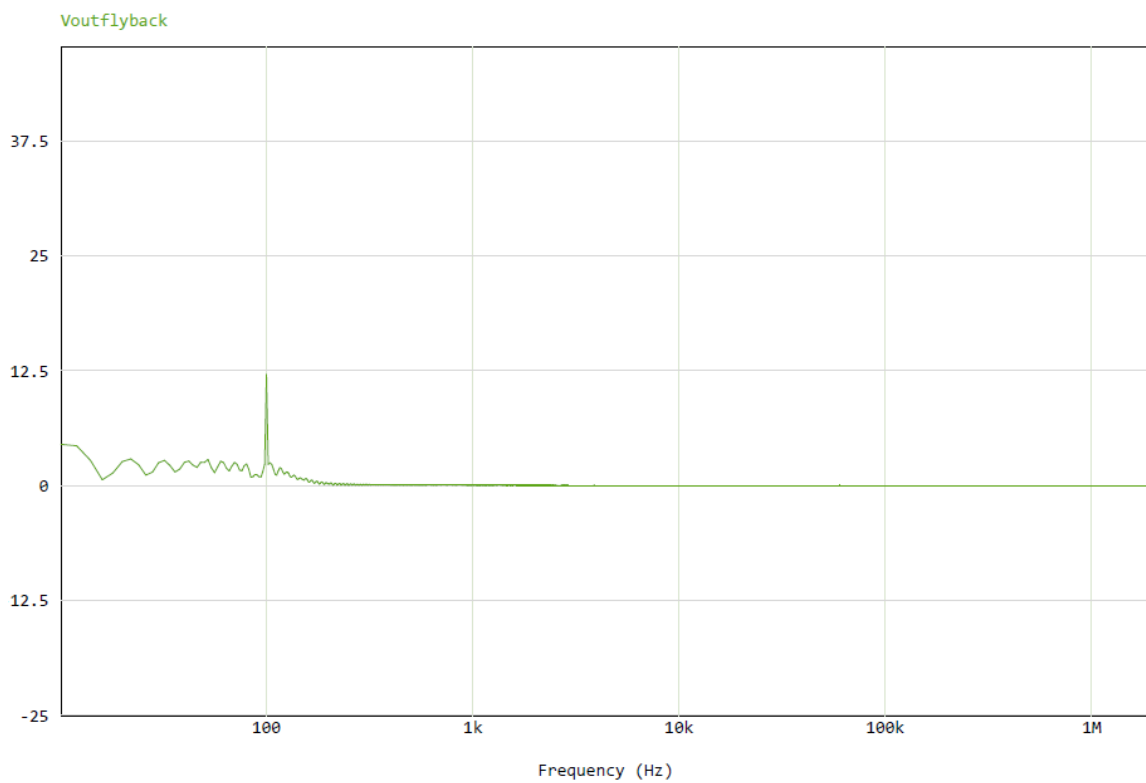


Figure 4.10 DC stage voltage spectral analysis (control strategy 2)

It must be noted that compensation value of current (or inductor current) in this system is much different than in case of proposed control and 3rd control strategy (Fig. 4.7). There is much less high frequency component in it. It could be justified by the fact that this strategy uses more filtered parameters than other strategies.

Fig. 4.9 shows us that current and voltage parameters on PV side are quite distorted, despite of facts that buffer and DC-link capacitances are relatively high.

Talking about the spectral analysis of filtered voltage parameter, we can see, that this control strategy provides better filtering option for both: 2nd harmonic and higher frequency components.

4.3 Experimental results of control strategy 3

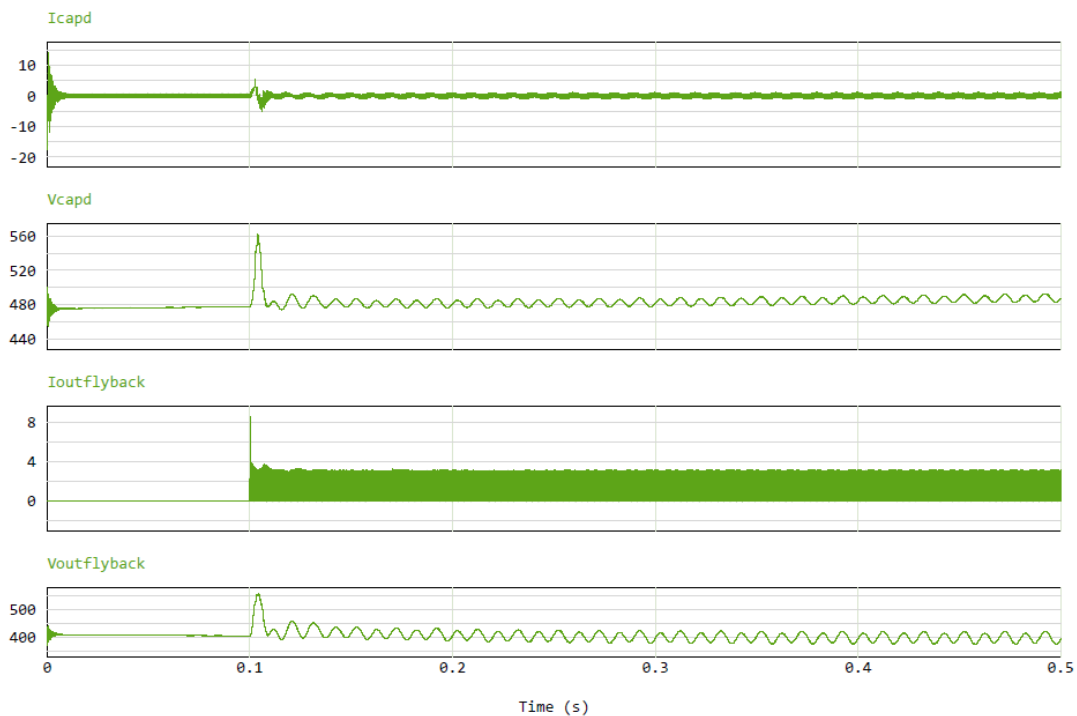


Figure 4.11 Active decoupling circuit and DC stage of inverter voltage and current values. As we can see from the Fig. 4.11, working mode of microinverter with active decoupling technique is the most stable of all the 3 reviewed strategies.

With this control, circuit reaches its steady state after 1 second of working. Voltage across capacitor is controlled to be 500V, this effect cannot be achieved within 0,5 second but is also achieved after 1 second.

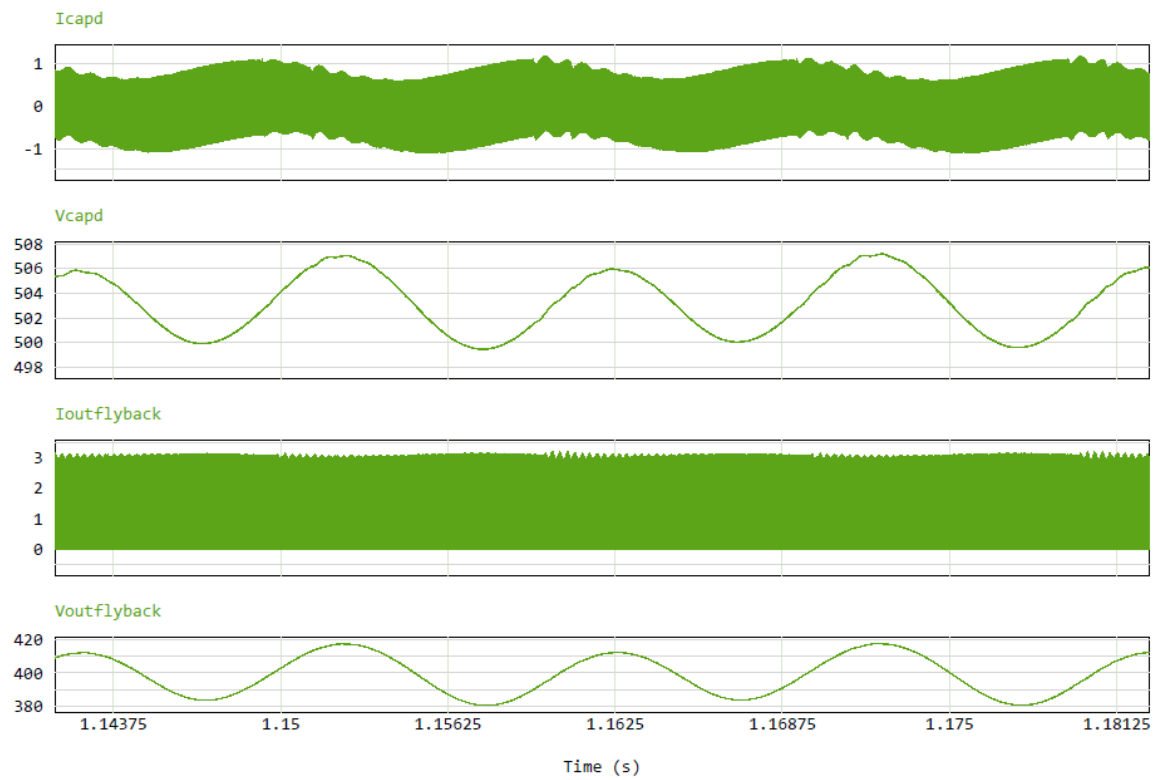


Figure 4.12 Active decoupling circuit and DC stage of inverter voltage and current values, zoomed

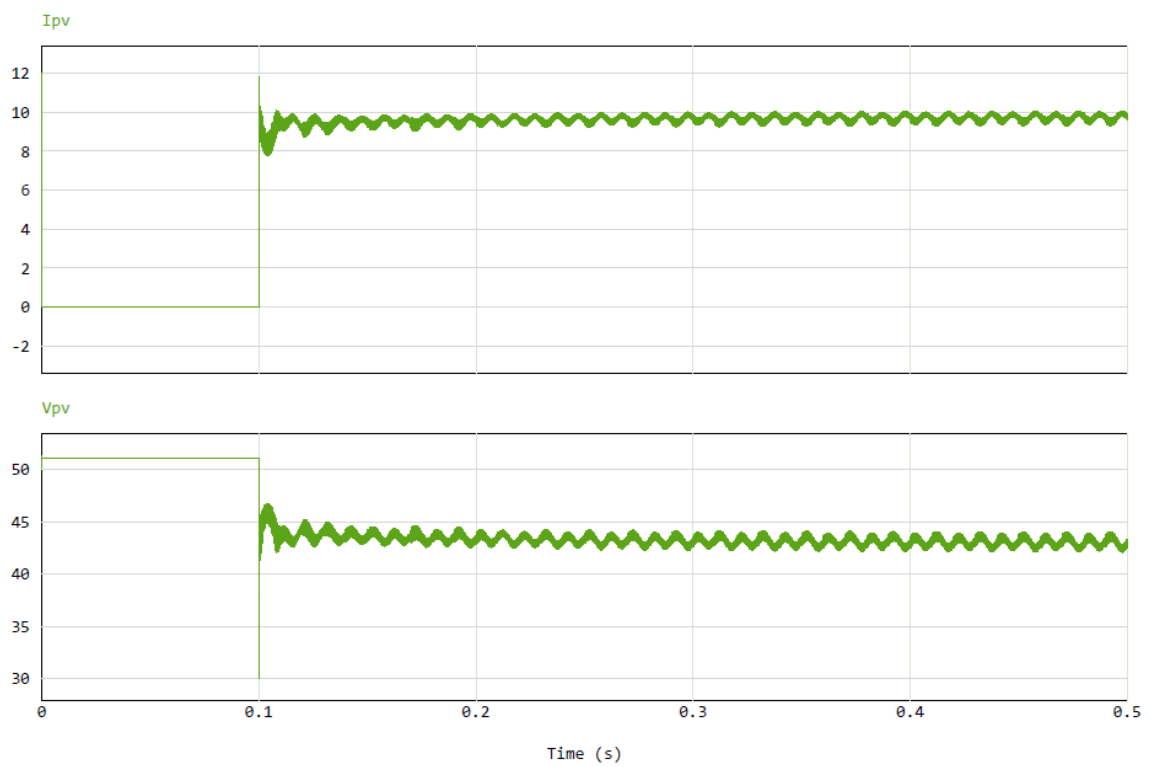


Figure 4.13 Voltage and current values on PV side (control strategy 3)

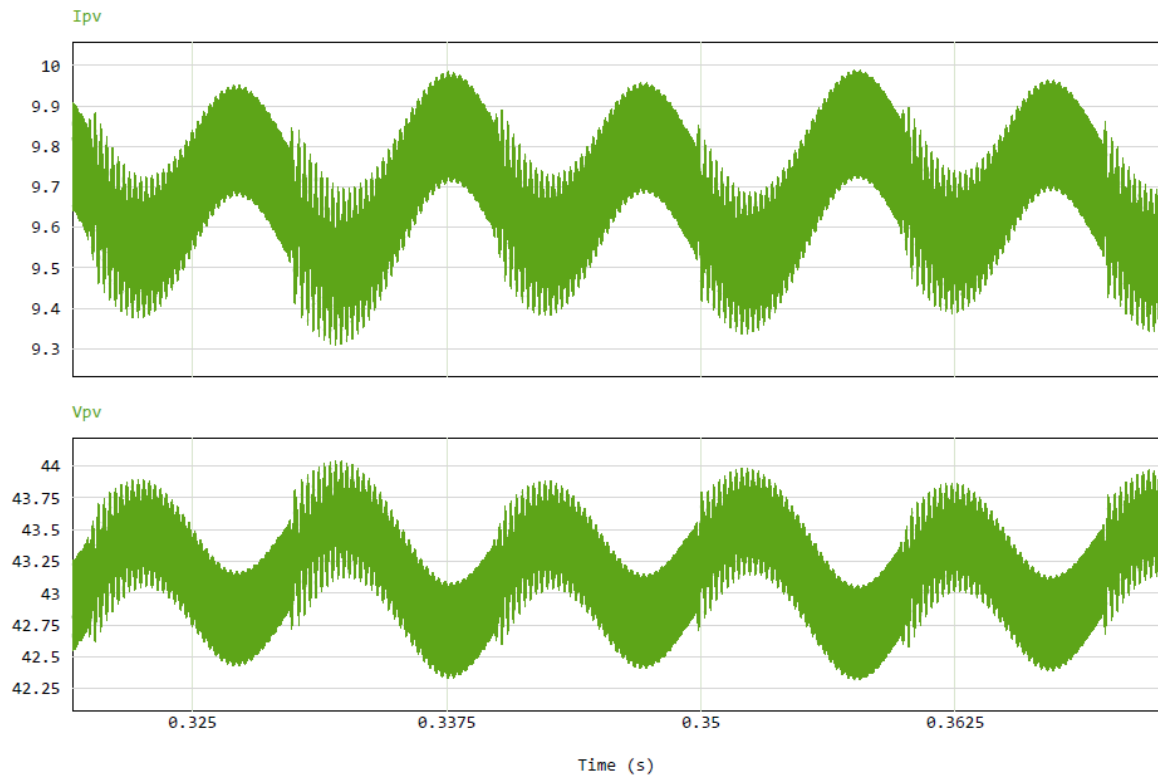


Figure 4.14 Voltage and current values on PV side, zoomed (control strategy 3)

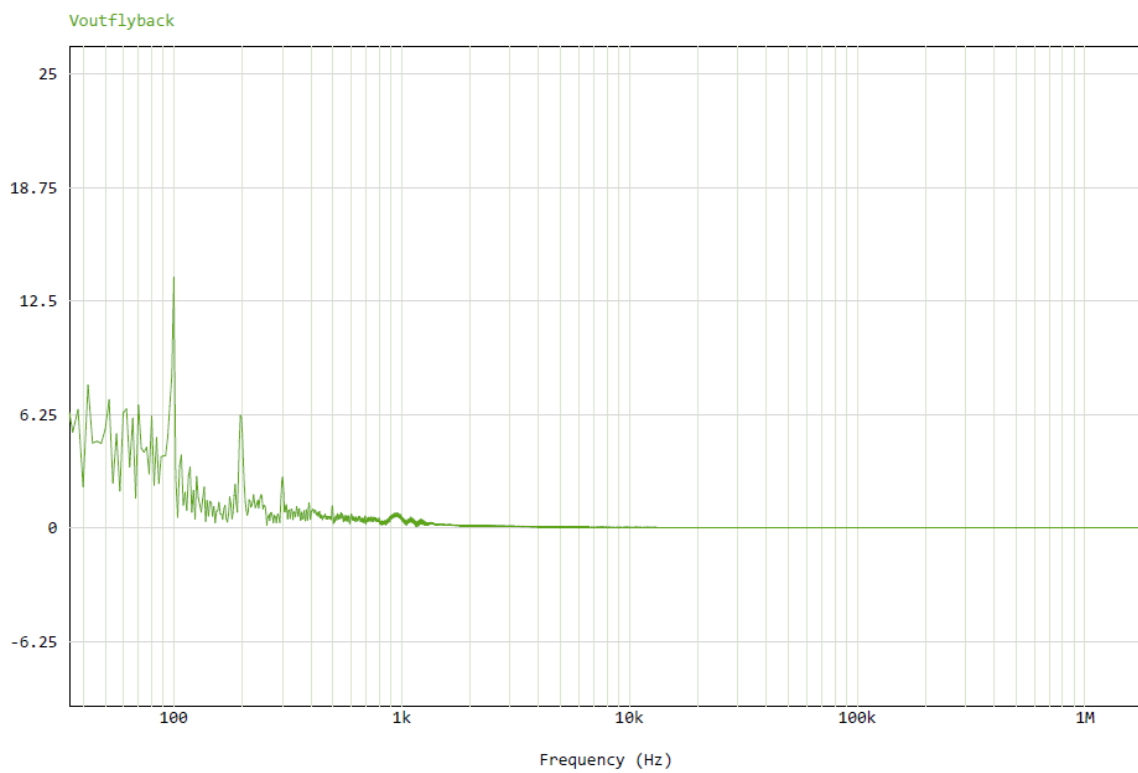


Figure 4.15 DC stage voltage spectral analysis (control strategy 2)

Experimental results of this control strategy are quite similar to other strategies. But in this case voltage across capacitor is better controlled and kept according to reference value.

Voltage and current values from PV side are less distorted than in case of 2nd control strategy but still more distorted than in case of proposed control. It could be due to fact that buffer and DC-link capacitors values are the higher.

According to spectral analysis (Fig. 4.15), filtering capability is similar to proposed strategy but worse than 2nd one. Second harmonic amplitude is made to be low, but 4th and 6th harmonics are still quite unfiltered. In this case high frequency switching parameter is completely filtered.

5. ANALYSIS OF SIMULATION RESULTS AND COMPONENTS SELECTION

As we have seen from the topic 4, all control strategies provide proper results. Proposed control strategy requires less capacitance in both: DC-link and buffer capacitors. But the disadvantage of proposed control is that inductor current and voltage across capacitor are quite high. As a result, volumes of components that will be selected, could be larger.

On opposite, control strategy 2 and 3 provides capability to work at smaller current and voltage values. But in those cases, capacitances of components are higher, it fact also affects the overall volume of the system.

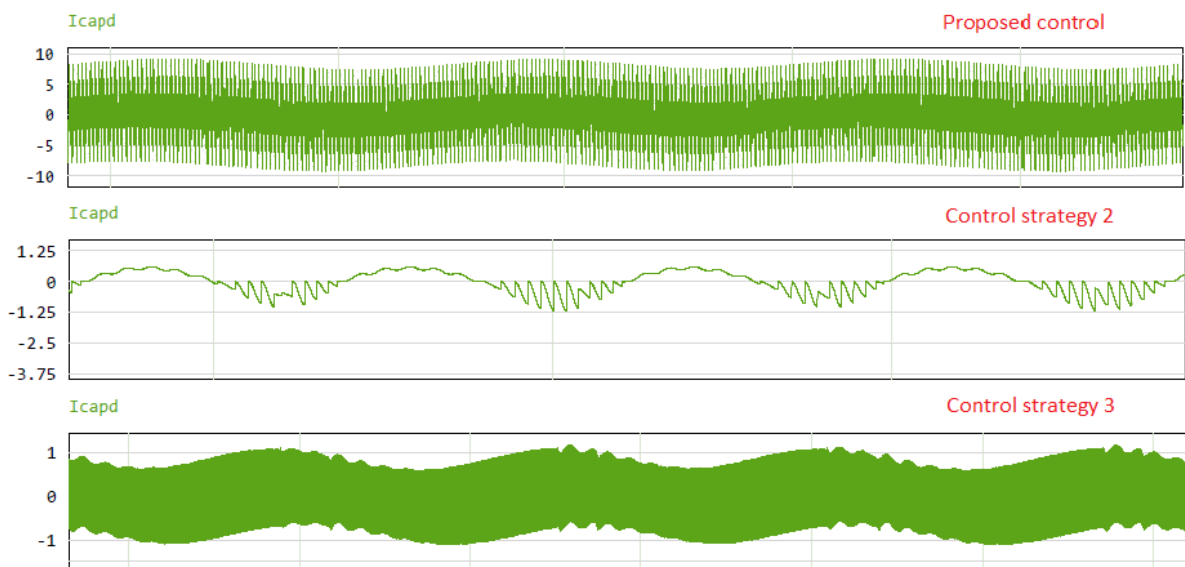


Figure 5.1. Active decoupling circuit inductor current.

On the figure 40 are shown active decoupling circuit inductor current values for all control methods. It can be seen that current value in control strategy 2 contains less high frequency components.

For proposed and 3rd control strategies there are similar current waves, but as it is seen, in proposed control the current value is the most distorted. Current distortion exceeds average value for more than 2 times.

Reviewing spectral analyses, it is obvious that all the 3 control methods are suitable for filtering 2nd harmonics, but control strategy 2 provides better result in filtering high frequency components.

Proposed control and 3rd control strategy provide similar good results, but in case of last reviewed control there are much larger DC-link and buffer capacitor values, so it could be also justified not by capability of control method but also by high capacitance.

Talking about final current and voltage values at PV side, it can be seen that despite the smaller capacitance, proposed control has less fluctuations and distortion than other control methods and therefore more suitable as a microinverter filtering unit. Proposed control also shows better results than passive decoupling with large capacitor. Results of other controls are similar to passive decoupling simulation results.

5.1 Components selection

As it was discussed before, range of suitable values for different components were calculated in the 2nd part of this thesis work. Final values were found by using try and error method in the 4th part of this research. In this part of work real existed components are chosen and their size parameters are defined.

Components for decoupling circuits are chosen according to calculated and experimentally found parameters. In tables 5.1-5.3 are shown chosen components and their volumes. From the tables 5.1-5.3 and figure 5.2 we can see that all reviewed control strategies provide better power density than passive decoupling technique because of significant reducing of capacitance.

Proposed control:

Table 5.1 Components and their volumes for proposed control. [46][47][48][49]

Type	Name	Size (L x W x H), mm	Size (D x H), mm	Volume, mm ³
Capacitor	BLH805K102A082	32x22x27	-	26048
Capacitor	DCP4G054006J	20x39x31.5	-	24885
Inductor	DKIH-3237-10D8	-	37x26	27955
MOSFET	IXTT10N100D2	4.9x13.8x15.85	-	1072

Control strategy 2:

Table 5.2 Components and their volumes for the control strategy 2. [46][50][51]

Type	Name	Size (L x W x H), mm	Size (D x H), mm	Volume, mm ³
Capacitor	DCP4H156007I	31x46x41.5	-	59179
Capacitor	DCP4G054006J	20x39x31.5	-	24885
Inductor	SC-02-08JS	-	26x12	6371
MOSFET	SiHB25N50E	4.06x8.38x9.65	-	328

Control strategy 3:

Table 5.3. Components and their volumes for the control strategy 3. [46][50][51]

Type	Name	Size (L x W x H), mm	Size (D x H), mm	Volume, mm ³
Capacitor	DCP4H158007I	46x41.5x37x5	-	59179
Capacitor	DCP4G056007G	20x39.5x41.5	-	32785
Inductor	SC-02-08JS	-	26x12	6371
MOSFET	SiHB25N50E	4.06x8.38x9.65	-	328

As it is seen, proposed control strategy provides better result in term of power density than other strategies and passive decoupling. Better power density is defined by low buffer capacitance. In case of proposed control, decoupling circuit is working at very high voltage and current values, this fact affects the overall volume because components have to withstand higher voltage and current and thus are over-dimensioned.

Passive decoupling:

Type	Name	Size (L x W x H), mm	Size (D x H), mm	Volume, mm ³
Capacitor	DCP4G062509H	44x55x57	-	141075

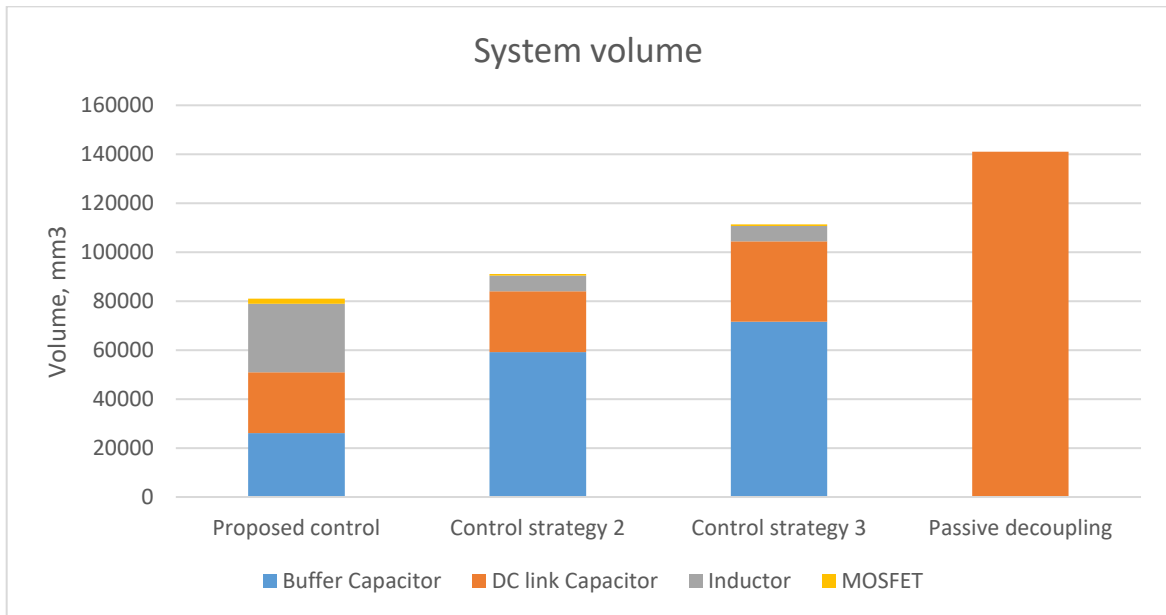


Figure 5.2 Comparison of reviewed control strategies and passive decoupling circuit volumes.

Components cost:

Table 5.4 Components cost (according to www.mouser.ee)

Component	Components cost, EUR			
	Proposed control	Control strategy 2	Control strategy 3	Passive decoupling
BLH805K102A082	4.98			
DCP4G054006J	10.92			
DKIH-3237-10D8	12.56			
IXTT10N100D2	35.38			
DCP4H156007I		13.02		

DCP4G054006J		10.92		
SC-02-08JS		3.07		
SiHB25N50E		6.84		
DCP4H158007I			16.23	
DCP4G056007G			14.18	
SC-02-08JS			3.07	
SiHB25N50E			6.84	
DCP4G062509H				43.79

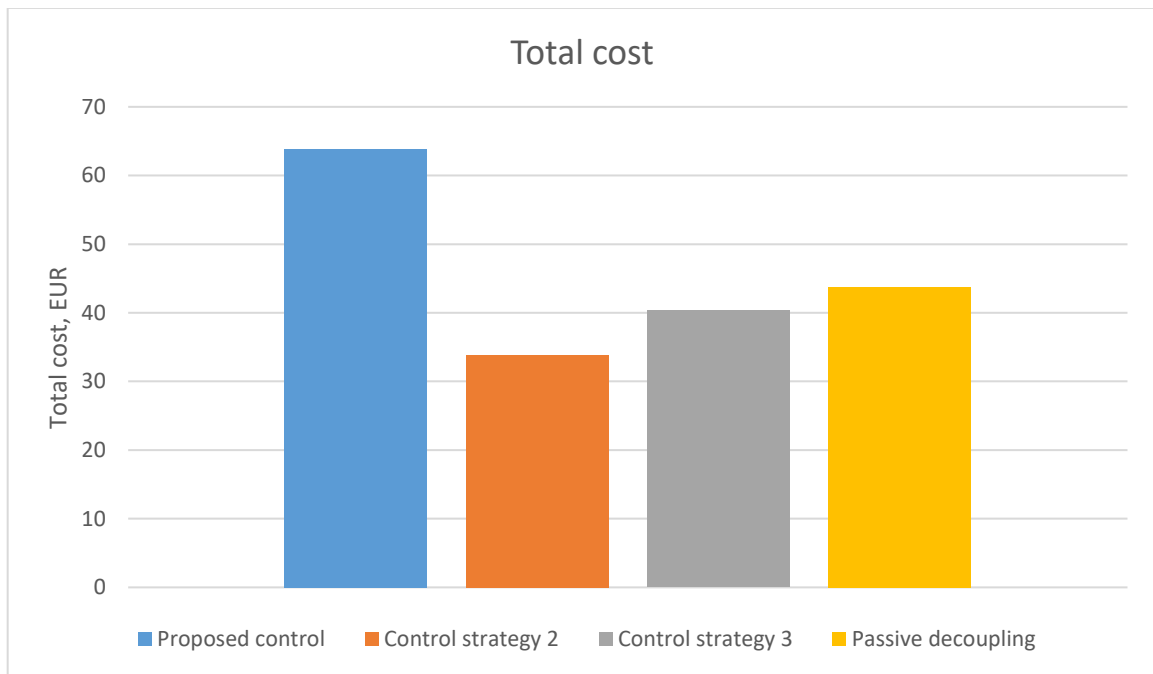


Figure 5.3 Comparison of components cost

As it can be seen from the figure 5.3, proposed control has the highest total cost of components. It is mainly due to the high cost of the MOSFET transistor that has to be able working with high voltage and current ratings.

It is also seen, that cost of passive decoupling component is relatively high and even exceeds the cost of components for 2nd and 3rd control strategies. Passive decoupling capacitor high cost is connected to the fact that it is oriented to be working at relatively high voltage level with relatively high capacitance, so by default not electrolytic but a film capacitor was chosen.

It must also be noted that the cost of the system does not always depend on the components' cost, but also the duration and cost of the design process must be taken into account. In the case of passive decoupling design process is much easier and takes less time, so overall cost could be also lower than for active decoupling techniques.

5.2 MOSFET power losses

In this topic MOSFET transistors losses will be reviewed and compared for each control method. In the table 5.4 parameters needed to calculate MOSFET power losses are shown. In must be noted, that voltage and current RMS values are obtained from the analysis tool of PSIM simulation software.

Table 5.5. MOSFET parameters

	Proposed control	Control strategy 2	Control strategy 3
	IXTT10N100D2	SiHB25N50E	SiHB25N50E
U_{DS}, V	920	406	501
$I_{D(MAX)}, A$	10	16	16
$I_{D(RMS)}, A$	5.5	0.6	0.5
f_{SW}, Hz	60000	60000	60000
$R_{DS(on)25^{\circ}C}, \Omega$	1.5	0.145	0.145
t_{off}, ns	33	57	57
t_{on}, ns	33	19	19
$T_{j(MAX)}, ^{\circ}C$	150	150	150

MOSFET losses mainly consist of **conduction** and **switching** losses.

5.2.1 Conduction losses calculation

Conduction losses refer to the amount of energy that is lost as heat as current passes through the channel between the drain and source terminals of the MOSFET. These losses occur due to the resistance of the channel, which causes some of the electrical energy to be dissipated as heat rather than being transmitted to the load.

As we can see from the equation 5.1, Conduction losses can be a significant factor in the overall power dissipation of a MOSFET, particularly in high-power applications where

large currents are involved. MOSFET conduction losses can be calculated using following equation [38]:

$$P_{CD} = R_{DS(on)} * I_{D(RMS)}^2 \quad (5.1)$$

For T=25°C following results are obtained:

Table 5.6. Calculated conduction losses for T=25°C

	Proposed control	Control strategy 2	Control strategy 3
	IXTT10N100D2	SiHB25N50E	SiHB25N50E
P_{CD}, W	45.375	0.052	0.036

Conduction losses for maximal allowed working temperature can be calculated using $R_{DS(on)}$ value that correspond to maximal temperature. $R_{DS(on)T_j}$ value can be calculated as follows:

$$R_{DS(on)T_j} = R_{DS(on)25^\circ C} + \left(1 + \frac{\alpha}{100}\right)^{T_j - 25^\circ C} \quad (5.2)$$

where α – temperature coefficient.

In this work corrected parameter $R_{DS(on)150^\circ C}$ are found from MOSFET datasheets as shown on Fig. 5.3.

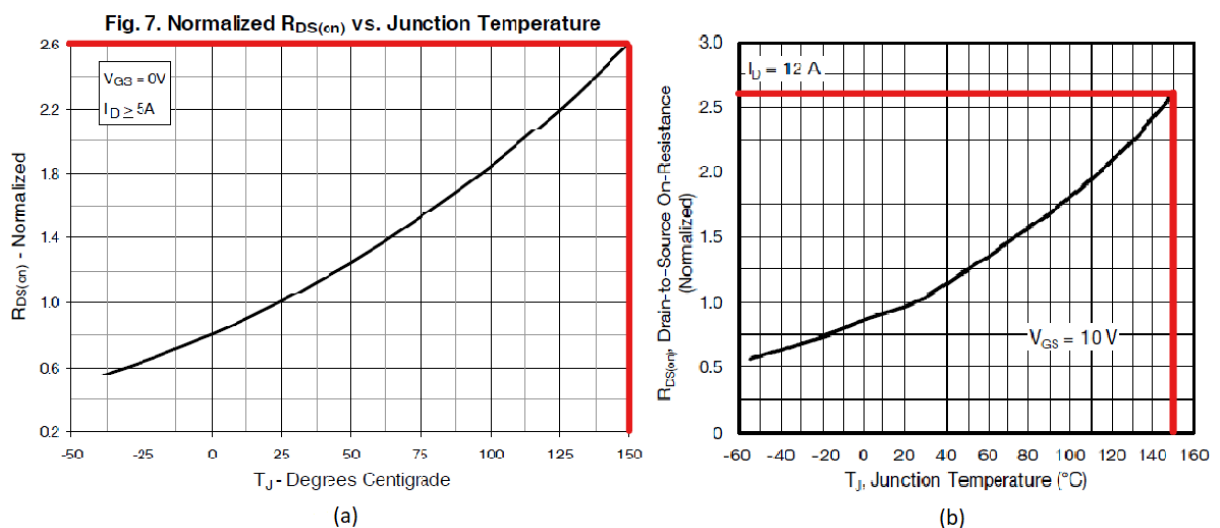


Figure 5.4. Corrected $R_{DS(on)}$ parameters found from datasheets. (a) - IXTT10N100D2, (b) - SiHB25N50E

For junction temperature T=150°C following results are obtained:

Table 5.7. Calculated conduction losses for T=150°C

	Proposed control	Control strategy 2	Control strategy 3
	IXTT10N100D2	SiHB25N50E	SiHB25N50E
P_{CD}, W	78.650	0.905	0.629

5.2.2 Switching losses calculations

Switching losses refer to the amount of energy that is lost during the process of turning a MOSFET on and off. When a MOSFET switches on or off, there is a brief period of time during which MOSFET internal parasitic capacitance needs to be loaded, leading to power dissipation in the device. As it can be seen from the equation 5.3, switching losses can be a significant factor in the overall power dissipation of a MOSFET, particularly in high-frequency switching applications where the device is turned on and off rapidly.

MOSFET switching losses can be calculated using following equation [39]:

$$P_{SW} = \frac{1}{2} * U_{DS} * I_{D(RMS)} * f_{SW} * (t_{on} + t_{off}) \quad (5.3)$$

Table 5.8 Calculated switching losses

	Proposed control	Control strategy 2	Control strategy 3
	IXTT10N100D2	SiHB25N50E	SiHB25N50E
P_{SW}, W	10.019	0.555	0.462

5.2.3 Analysis of calculated losses

As it can be seen from topics 5.2.1 and 5.2.2, conduction and switching losses in proposed control strategy are significantly higher than for other strategies. This fact is connected to higher voltage and current values in the active power decoupling circuit. As we can see from the equations 5.1 and 5.3, main parameters that define losses are voltage and current values, because switching frequency are the same and t_{on} , t_{off} parameters could be also assumed to be same because of relatively small difference between them.

Talking about conduction losses, their value highly depends on the $R_{DS(on)}$ value. $R_{DS(on)}$ is drain-source on-resistance and it is a parameter used to describe the resistance

between the drain and source terminals of a MOSFET when it is in its "ON" state. Its value depends on many factors such as physical dimensions of MOSFET, doping concentration of the semiconductor layers, and the operating temperature etc.

For a IXTT10N100D2 MOSFET, its $R_{DS(on)}$ value is 10 times higher than in SiHB25N50E. This difference can be justified by larger size of MOSFET, because it must be capable to work at higher voltage and current. It must be noted, that for maximal junction temperature the $R_{DS(on)}$ value for aforementioned types of MOSFET is almost the same.

Comparing conduction and switching losses, it is seen, that conduction losses higher for the IXTT10N100D2, because it works at relatively low frequency but relatively high voltage and current. For SiHB25N50E switching and conduction losses seems to be similar and depending on junction temperature conduction loss could be slightly lower or higher than switching one.

SUMMARY

In this thesis work, various topics were discussed and reviewed. The theoretical part of the work provided sufficient information about microinverters and their topologies, passive and active decoupling circuits, and the evaluation of Fast Fourier transform for estimating different frequency components in measured voltage or current signals.

The practical part of the thesis work focused on discussing selected microinverter topology, active power decoupling circuit, proposed control, existing control strategies for comparison, and the evaluation of FFT for analysing proposed and selected control strategies in terms of different harmonics in the DC-stage of the microinverter. The practical part also included a discussion of the results of modulating different control strategies, their suitability for filtering different frequency components, the overall volume of the system, and the system cost.

The thesis work compares three control strategies for a microinverter filtering unit in terms of component volume, power density, cost, and losses. The proposed control strategy requires less capacitance in the DC-link and buffer capacitors but has high inductor current and voltage across the capacitor, resulting in larger component volumes. Control strategies 2 and 3 work at smaller current and voltage values, but have higher capacitances, affecting the overall volume of the system.

Spectral analyses show that all three control methods are suitable for filtering 2nd harmonics, but control strategy 2 provides better results in filtering high-frequency components. The proposed control strategy has less fluctuation and distortion at the PV side, making it more suitable as a microinverter filtering unit than other strategies.

From the point of view of chosen components, it is seen that all reviewed control strategies provide better power density than passive decoupling technique due to significant capacitance reduction. The proposed control strategy provides better power density than other strategies or passive decoupling due to smaller capacitance. The total cost of components for proposed control technique is higher mainly due to the high cost of MOSFET transistors, but still competitive with other strategies or passive decoupling.

Conduction and switching losses were also calculated and reviewed in this thesis work and it can be stated, that in the proposed control strategy those losses significantly higher than for other strategies due to higher voltage and current values in the active power decoupling circuit. In case of conduction losses that depend also on the $R_{DS(on)}$ value of the MOSFET, it is obvious that this value is much higher than for smaller

MOSFET because of physical size of selected switching device. Switching and conduction losses for SiHB25N50E seem to be similar, and depending on the junction temperature, conduction losses could be slightly lower or higher than switching losses.

To sum up the final choice of decoupling type and control strategy depends on the requirements:

- Proposed control could be chosen when the low power density is a crucial factor and slightly higher cost is not a problem. Another advantage is that the control scheme is relatively easy and applicable in a large range of tasks, but working at higher voltage and current values must be allowed.
- Control strategy 2 is the best choice for filtering higher harmonics. It also has the lower cost and could be chosen if relatively high power density and low cost is requested. Main disadvantage of 2nd control strategy is its difficult and not very reliable control scheme.
- Control strategy 3 has the worst power density, relatively high cost and difficult control scheme. This control scheme doesn't have any advantages over other control strategies and is not a good choice as a filter.
- Passive decoupling could be chosen if the overall simplicity of the system is required, and high power density is not a crucial factor.

As a plan for the future research and improvement of proposed control, the proper control of current and voltage values must be reviewed and implemented to decrease the overall volume and the cost of the system.

KOKKUVÕTE

Selles lõputöös käsitleti ja analüüsiti erinevaid teemasid. Töö teoreetiline osa pakkus piisavalt teavet mikroinverterite ja nende topoloogiatega, passiivsete ja aktiivsete eraldamisahelate ning FFT hindamise kohta erinevate sageduskomponentide hindamiseks mõõdetud pingepinge- või voolusignaalis.

Lõputöö praktiline osa keskendus valitud mikroinverteri topoloogia, aktiivse eraldamisahela, pakutud juhtimise, olemasolevate juhtimisstrateegiatega võrdlemise ja FFT hindamisele, et analüüsida pakutud ja valitud juhtimisstrateegiatega sobivust mikroinverteri alalisvoolu staadiumis erinevate harmooniliste komponentide suhtes. Praktiline osa hõlmas ka tulemuste arutelu erinevate juhtimisstrateegiatega modulatsiooni sobivuse, erinevate sageduskomponentide filtreerimise sobivuse, süsteemi üldmahu ja süsteemi maksumuse osas.

Lõputöö võrdleb kolme juhtimisstrateegiat mikroinverteri filtreerimisüksuse jaoks komponentide mahutavuse, võimsustiheduse, maksumuse ja kadude osas. Pakutud juhtimisstrateegia nõuab vähem mahtuvust alalisvoolu ahelas ja puhvermahtuvust, kuid sellel on suurem vool ja kondensaatori pingepinge, mis suurendab komponentide mahtu. Juhtimisstrateegiad 2 ja 3 töötavad väiksemate voolu- ja pingepingeväärtustega, kuid neil on suuremad mahtuvused, mõjutades süsteemi üldmahtu.

Spektraalanalüüsid näitavad, et kõik kolm juhtimismeetodit sobivad 2. harmooniliste komponentide filtreerimiseks, kuid juhtimisstrateegia 2 annab paremaid tulemusi kõrgsageduslike komponentide filtreerimisel. Pakutud juhtimisstrateegial on vähem kõikumisi ja moonutusi PV-poolel, mistõttu on see teistest strateegiatest sobivam mikroinverteri filteriks.

Komponentide valiku seisukohalt on näha, et kõik vaadeldud juhtimisstrateegiad pakuvad võimsustihedust, mis on parem kui passiivse lahtisidumise puhul, tänu olulisele mahtuvuse vähendamisele. Pakutud juhtimisstrateegia pakub paremat võimsustihedust kui teised strateegiad või passiivne lahutamise tänu väiksemale mahtuvusele. Pakutava juhtimisstrateegia komponentide kogukulu on kõrgem peamiselt MOSFET transistoride kõrge hinna tõttu, kuid see on siiski konkurentsivõimeline võrreldes teiste strateegiatega või passiivse lahutusega.

Töös arutati ja vaadeldi ka juhtimiskadusid ning võib öelda, et pakutava juhtimisstrateegia korral on need kaod teiste strateegiatega võrreldes märkimisväärselt suuremad kõrgemate pingete ja voolude tõttu. Juhtimiskadude puhul, mis sõltuvad ka

MOSFET-i $R_{DS(on)}$ väärtusest, on ilmne, et see väärtus on valitud lülitusseadme füüsilise suuruse tõttu palju suurem kui väiksemate MOSFET-ide puhul. Lülituskaod SiHB25N50E puhul tunduvad sarnased juhtimiskadudega ning sõltuvalt ühenduse temperatuurist võivad juhtimiskaod olla veidi väiksemad või suuremad kui lülituskaod.

Kokkuvõttes sõltub lahutustüübi ja juhtimisstrateegia lõplik valik nõuetest, mis on vajalikud süsteemi nõuetekohaseks tööks:

- Pakutud juhtimisstrateegiat võib valida siis, kui madal võimsustihedus on oluline tegur ja veidi kõrgem kulu pole probleem. Teine eelis on see, et juhtimisskeem on suhteliselt lihtne ja rakendatav suurel hulgal ülesannetes, kuid töötamine kõrgema pingega ja voolu juures peab olema lubatud.
- Juhtimisstrateegia 2 on parim valik kõrgemate harmooniliste komponentide filtreerimiseks. Sellel on ka madalam hind ja seda saab valida, kui nõutakse suhteliselt suurt võimsustihedust ja madalat hinda. Peamine 2. juhtimisstrateegia puudus on selle keeruline ja mitte eriti usaldusväärne juhtimisskeem.
- Juhtimisstrateegia 3-I on kõige halvem võimsustihedus, suhteliselt kõrge hind ja keeruline juhtimisskeem. Sellel juhtimisskeemil pole teiste juhtimisstrateegiate ees eeliseid ja see pole filtrina hea valik
- Kui süsteemi üldine lihtsus on oluline ja kõrge võimsustihedus pole otsustav tegur, võib valida passiivse eraldamise.

Tulevase uurimistöö raames tuleb uurida ja rakendada pakutud juhtimise struktuuri juures parema pinge ja voolu juhtimise, et vähendada süsteemi üldmahtu ja kulusid.

LIST OF REFERENCES

- [1] Ö. Celik, A. Teke, A. Tan, "Overview of micro-inverters as a challenging technology in photovoltaic applications," *Renewable and Sustainable Energy Reviews*, vol. 82, 2018, doi: 10.1016/j.rser.2017.10.024.
- [2] A. Razi, M. N. Hidayat, M. N. Seroji, "Microinverter Topology based Single-stage Grid-connected Photovoltaic System: A Review," *Indonesian Journal of Electrical Engineering and Computer Science*, vol. 11, pp 645-651, 2018, doi: 10.11591/ijeecs.v11.i2.pp645-651.
- [3] A. S. Morsy, P. N. Enjeti, "Comparison of Active Power Decoupling Methods for High-Power-Density Single-Phase Inverters Using Wide-Bandgap FETs for Google Little Box Challenge," *IEEE Journal of Emerging and Selected Topics in Power Electronics*, vol. 4, no. 3, pp. 790-798, 2016, doi: 10.1109/JESTPE.2016.2573262.
- [4] H. Hu, S. Harb, N. Kutkut, I. Batarseh, Z. J. Shen, "Power decoupling techniques for micro-inverters in PV systems-a review," 2010 IEEE Energy Conversion Congress and Exposition, Atlanta, GA, USA, 2010, pp. 3235-3240, doi: 10.1109/ECCE.2010.5618285.
- [5] O. G. Gnonhoue, A. Velazquez-Salazar, E. David, I. Preda, "Review of Technologies and Materials Used in High-Voltage Film Capacitors," *Polymers*, vol. 13, 2021, doi: 10.3390/polym13050766
- [6] V. Michal, "Switched-Mode Active Decoupling Capacitor Allowing Volume Reduction of the High-Voltage DC Filters," *IEEE Transactions on Power Electronics*, vol. 31, no. 9, pp. 6104-6111, 2016, doi: 10.1109/TPEL.2015.2500920.
- [7] Y. Zhang, J. Xiong, P. He, S. Wang, "Review of power decoupling methods for micro-inverters used in PV systems," *Chinese Journal of Electrical Engineering*, vol. 4, no. 4, pp. 26-32, 2018, doi: 10.23919/CJEE.2018.8606786.
- [8] Y. Sun, Y. Liu, M. Su, W. Xiong, J. Yang, "Review of Active Power Decoupling Topologies in Single-Phase Systems," *IEEE Transactions on Power Electronics*, vol. 31, no. 7, pp. 4778-4794, July 2016, doi: 10.1109/TPEL.2015.2477882.
- [9] X. Cao, Q. -C. Zhong, W. -L. Ming, "Ripple Eliminator to Smooth DC-Bus Voltage and Reduce the Total Capacitance Required," *IEEE Transactions on Industrial Electronics*, vol. 62, no. 4, pp. 2224-2235, 2015, doi: 10.1109/TIE.2014.2353016.

- [10] J. Zhang, H. Ding, B. Wang, X. Guo, and S. Padmanaban, "Active Power Decoupling for Current Source Converters: An Overview Scenario," *Electronics*, vol. 8, no. 2, p. 197, 2019, doi: 10.3390/electronics8020197.
- [11] A. R. Gautam, D. M. Fulwani, R. R. Makineni, A. K. Rathore, D. Singh, "Control Strategies and Power Decoupling Topologies to Mitigate 2ω -Ripple in Single-Phase Inverters: A Review and Open Challenges," *IEEE Access*, vol. 8, pp. 147533-147559, 2020, doi: 10.1109/ACCESS.2020.3015315.
- [12] D. Pan, X. Ruan, X. Wang, H. Yu, Z. Xing, "Analysis and Design of Current Control Schemes for LCL-Type Grid-Connected Inverter Based on a General Mathematical Model," *IEEE Transactions on Power Electronics*, vol. 32, no. 6, pp. 4395-4410, 2017, doi: 10.1109/TPEL.2016.2602219.
- [13] Z. Qin, Y. Tang, P. C. Loh, F. Blaabjerg, "Benchmark of AC and DC Active Power Decoupling Circuits for Second-Order Harmonic Mitigation in Kilowatt-Scale Single-Phase Inverters," *IEEE Journal of Emerging and Selected Topics in Power Electronics*, vol. 4, no. 1, pp. 15-25, 2016, doi: 10.1109/JESTPE.2015.2490199.
- [14] U. Siddique, M. Y. Mahmoud, S. Tahar, "Formal Analysis of Discrete-Time Systems using z-Transform," *IFCoLog Journal of Logics and their Applications*, vol. 5, 2018.
- [15] L. Saribulut, A. Teke, M. Tümai, "Fundamentals and literature review of Fourier transform in power quality issues," *Journal of Electrical and Electronics Engineering Research*, 2013.
- [16] M. A. G. de Brito, L. Galotto, L. P. Sampaio, G. d. A. e Melo, C. A. Canesin, "Evaluation of the Main MPPT Techniques for Photovoltaic Applications," *IEEE Transactions on Industrial Electronics*, vol. 60, no. 3, pp. 1156-1167, 2013, doi: 10.1109/TIE.2012.2198036.
- [17] R. Faranda, S. Leva, "Energy comparison of MPPT techniques for PV Systems," *Journal of Electromagnetic Analysis and Applications*, vol. 3, 2008.
- [18] D. F. S. Fernandes, R. F. O. Costa, L. A. M. Barros, D. Pedrosa, J. L. Afonso, J. G. Pinto, "A Comprehensive Comparison of Voltage and Current Control Techniques for Three-Phase VSI Converters. Sustainable Energy for Smart Cities," *SESC 2021. Lecture Notes of the Institute for Computer Sciences, Social Informatics and Telecommunications Engineering*, vol 425, 2022.

- [19] M. Leso, J. Žilkova, M. Biroš, P. Talian, "Survey of control methods for DC-DC converters," *Acta Electrotechnica et Informatica*, 2018.
- [20] Er. S. S. Deshmukh, Er. S. S. Khule, "Different Control Strategies for Power Control of Voltage Source Converters in a Microgrid," *International Research Journal of Engineering and Technology*, vol. 5, 2018.
- [21] S. A. Yaqoob, A. Obed, "Photovoltaic flyback micro-inverter with power decoupling technique," *Indonesian Journal of Electrical Engineering and Computer Science*, vol. 15, 2019.
- [22] D. Elangovan, G. Arunkumar, V. Indragandhi, S. Venkatesh, R. Kannan, "DESIGN AND ANALYSIS OF FLYBACK MICRO INVERTER FOR INTEGRATION OF FUEL CELLS WITH SINGLE PHASE GRID," *International Journal of Mechanical Engineering and Technology (IJMET)*, vol. 8, 2017.
- [23] D. Mathew, C. N. Rani, "Investigation of single-stage transformerless buck-boost microinverters," *IET Power Electronics*, vol. 13, 2020, doi: 10.1049/iet-pel.2019.1237.
- [24] D. Mathew, C. N. Rani, Y. Wong, K. Busawon, "Single-Stage Microinverter with Current Sensorless Control for BIPV System," *IET Research Journals*, 2015, doi: 10.1049/rpg2.12177.
- [25] D. Mathew, M. E. Farrag, R. C. Naidu, R. K. Muthu, A. Sivaprakasam, "Buck-Boost Single-Stage Microinverter for Building Integrated Photovoltaic Systems. *Energies*, vol. 14, 2021, doi: 10.3390/en14237854.
- [26] Z. E. T. Ternifi, P. Petit, G. Bachir, M. Aillerie, "New Topology of Photovoltaic Microinverter based on Boost converter," *Energy Procedia*, vol. 119, 2017, doi: 10.1016/j.egypro.2017.07.106
- [27] D. Lopez-Caiza, H. Renaudineau, N. Muller, F. Flores-Bahamonde, S. Kouro, J. Rodriguez, "Dual-Boost Inverter for PV Microinverter Application—An Assessment of Control Strategies," *Applied Sciences*, 2022, doi: 10.3390/app12125952
- [28] D. Petreus, S. Daraban, I. Ciocan, T. Patarau, C. Morel, "Low-cost single stage micro-inverter with MPPT for grid connected applications," *Solar Energy*, vol. 92, 2013, doi: 10.1016/j.solener.2013.03.016
- [29] M. Qiu, P. Wang, H. Bi, Z. Wang, "Active Power Decoupling Design of AC-DC Converter for On-board Chargers," 2019 22nd International Conference on Electrical

Machines and Systems (ICEMS), Harbin, China, 2019, pp. 1-5, doi: 10.1109/ICEMS.2019.8922067.

[30] S. Sadrian, J. Wang, "Buck-Plus-Unfolder as the Superior Active Power Decoupling Solution for 400 Vdc/kW-Level Applications," *IEEE Open Journal of Power Electronics*, vol. 1, pp. 260-272, 2020, doi: 10.1109/OJPEL.2020.3010830.

[31] X. Cao, Q. -C. Zhong, W. -L. Ming, "Ripple Eliminator to Smooth DC-Bus Voltage and Reduce the Total Capacitance Required," *IEEE Transactions on Industrial Electronics*, vol. 62, no. 4, pp. 2224-2235, 2015, doi: 10.1109/TIE.2014.2353016.

[32] X. Cao, Q. -C. Zhong, W. -L. Ming, "Analysis and Control of Ripple Eliminators in DC Systems," 2014 Sixth Annual IEEE Green Technologies Conference, Corpus Christi, TX, USA, 2014, pp. 29-36, doi: 10.1109/GREENTECH.2014.23.

[33] H. Afshari, O. Husev, D. Vinnikov, O. Matiushkin, N. V. Kurdkandi, "Comparison of Grid-Connected Flyback-based Microinverter with Primary and Secondary Side Decoupling Approach," 2022 IEEE 63th International Scientific Conference on Power and Electrical Engineering of Riga Technical University (RTUCON), Riga, Latvia, 2022, pp. 1-6, doi: 10.1109/RTUCON56726.2022.9978855.

[34] H. Watanabe, J. -i. Itoh, Q. Roudier, "Single-phase power decoupling technique utilizing Hybrid method with passive and active power decoupling," 2018 IEEE International Power Electronics and Application Conference and Exposition (PEAC), Shenzhen, China, 2018, pp. 1-6, doi: 10.1109/PEAC.2018.8590577.

[35] Z. Kong, X. Huang, Z. Wang, J. Xiong, K. Zhang, "Active Power Decoupling for Submodules of a Modular Multilevel Converter," *IEEE Transactions on Power Electronics*, vol. 33, no. 1, pp. 125-136, 2018, doi: 10.1109/TPEL.2017.2661539.

[36] U. Drogenik, G. Laimer, J. Kolar, "Theoretical converter power density limits for forced convection cooling," ETH-Zentrum, Zurich, Switzerland, 2005.

[37] Y. Xiong, S. Sun, H. Jia, P. Shea, Z. John Shen, "New Physical Insights on Power MOSFET Switching Losses," *IEEE Transactions on Power Electronics*, vol. 24, no. 2, pp. 525-531, 2009, doi: 10.1109/TPEL.2008.2006567.

[38] G. Lakkas, "MOSFET power losses and how they affect power-supply efficiency. Analog Applications Journal," *Analog Application Journal*, Texas Instruments, 2016.

- [39] Y. Xiong, S. Sun, H. Jia, P. Shea, Z. John Shen, "New Physical Insights on Power MOSFET Switching Losses," *IEEE Transactions on Power Electronics*, vol. 24, no. 2, pp. 525-531, 2009, doi: 10.1109/TPEL.2008.2006567.
- [40] W. J. Sarjeant, J. Zirnheld, F. W. MacDougall, "Capacitors," *IEEE Transactions on Plasma Science*, vol. 26, no. 5, pp. 1368-1392, 1998, doi: 10.1109/27.736020.
- [41] W. J. Sarjeant, D. T. Staffiere, "A report on capacitors," *Proceedings of Applied Power Electronics Conference. APEC '96, San Jose, CA, USA, 1996*, pp. 12-17 vol.1, doi: 10.1109/APEC.1996.500415.
- [42] C. Reynolds, "Tantalum Capacitor Technology: Options for high-temperature and harsh-environment applications," *IEEE Power Electronics Magazine*, vol. 4, no. 1, pp. 43-47, 2017, doi: 10.1109/MPEL.2016.2642280.
- [43] P. Duhamel, M. Vetterli, "Fast Fourier transforms: A tutorial review and a state of the art," *Signal Processing*, vol. 19, no. 4, pp. 259-299, 1990, doi: 10.1016/0165-1684(90)90158-U.
- [44] R. N. Bracewell, "The Fourier Transform," *Scientific American*, pp. 86-95, 1989.
- [45] C. S. H. Kaushik, T. Gautam, V. Elamaran, "A tutorial review on discrete Fourier transform with data compression application," *2014 International Conference on Green Computing Communication and Electrical Engineering (ICGCCEE), Coimbatore, India, 2014*, pp. 1-6, doi: 10.1109/ICGCCEE.2014.6922210.
- [46] WIMA, "WIMADC-LINKMKP 4," 2021. [Online]. Available: https://www.mouser.ee/datasheet/2/440/e_WIMA_DC_Link_MKP_4-1139924.pdf [Accessed 14.05.2023].
- [47] CDE Cornell Dubilier, "Type BLH, DC Link Capacitors for Harsh Environments," 2021. [Online]. Available: <https://www.mouser.ee/datasheet/2/88/BLH-3081877.pdf> [Accessed 14.05.2023].
- [48] Schurter, "Compensated High Current Choke, 1-phase". [Online]. Available: https://www.mouser.ee/datasheet/2/358/typ_DKIH_1-1276015.pdf [Accessed 14.05.2023].
- [49] IXYS, "Depletion Mode MOSFET," 2017. [Online]. Available: https://www.mouser.ee/datasheet/2/240/ixys_s_a0003807242_1-2272645.pdf [Accessed 14.05.2023].

[50] KEMET, "Common Mode SC Coils, SC-JS Series, Terminal Base Type," 2019. [Online]. Available: https://www.mouser.ee/datasheet/2/212/1/KEM_LF0009_SC-JS-1104536.pdf [Accessed 14.05.2023].

[51] Vishay Siliconix, "E Series Power MOSFET," 2015. [Online]. Available: <https://www.vishay.com/docs/91646/sihb25n50e.pdf> [Accessed 14.05.2023].

[52] M. A. Chewale, V. B. Savakhande, H. T. Jadhav, "An interleaved flyback inverter for grid connected photovoltaic systems," 2017 International Conference on Circuit, Power and Computing Technologies (ICCPCT), Kollam, India, 2017, pp. 1-7, doi: 10.1109/ICCPCT.2017.8074270.